INFLUENCE OF PHONON MODES ON THE THERMAL CONDUCTIVITY OF SINGLE-WALL, DOUBLE-WALL, AND FUNCTIONALIZED CARBON NANOTUBES

By

EBONEE ALEXIS WALKER

Dissertation

Submitted to the Faculty of the

Graduate School of Vanderbilt University

in partial fulfillment of the requirements

for the degree of

DOCTOR OF PHILOSOPHY

in

Interdisciplinary Materials Science

May, 2012

Nashville, Tennessee

APPROVED:

Professor D. Greg Walker

Professor Richard Mu

Professor Clare M. McCabe

Professor Deyu Li

Professor Keivan G. Stassun

Professor Norman H. Tolk

To Mama Jo—who else?

ACKNOWLEDGEMENTS

Trust in the Lord with all your heart and lean not on your own understanding

—Proverbs 3:5

I thank God and Jesus Christ for my endurance during these last five and a half years. I do at times wonder how my life would be different if I had moved to Chicago and become a nuclear reactor inspector, as opposed to taking on an unknown course of study with little to go on other than my perseverance; but I trust that there is some bigger purpose in my life that is better served by me having completed this process. I will not pretend to understand what that purpose may be; but right now, I will take solace in having conquered every person and contrived task that sought to break my spirit. I am more than a conqueror.

I say thank you to everyone who offered encouragement. My mother, especially, gets a big thank you, since she had to listen to my ramblings about carbon nanotubes and thermal conductivity, as well as my rants about injustices I routinely experienced. My cheerleading section is my Walker, Cargle, and Cox families, as well as the Mt. Calvary Baptist Church family; there was never a lack of interest in my progress nor a lack of encouragement sent out. I have to mention my grandmother, Annie Lee Walker, who passed away shortly after I began graduate school—though I have learned many things, I have never forgot what she told me and never found any of it to be untrue.

Of course, graduate school is a long arduous journey and it would be that much harder if I had to go it alone—but I did not. I want to give my sincere appreciation to

fellow my graduate students. Some that I have known since I showed up back in August of 2006, like Desmond Campbell, Julia Bodnarik, and Dawit Jowhar—I extend congratulations to you all. Others—like Lucy Lu and Marquicia Pierce—I came to know through groups like Toastmasters, GSC, or OBGAPS, because graduate students can have a life. I cannot say enough about the encouragement I received from those who completed their studies before me; they never let me get down or believe I would do anything other succeed, so thanks go to Paula Hemphill, Wole Amusan, Jonathan Hunter, Saad Hasan, and Lidell Evans. I have to give a really special thanks and congratulations to John Rigueur, who decided to team up with me to knock our Ph.D.'s out together—well, we did it Dr. Rigueur! I do not plan to let the gift of encouragement stop with me, but rather I plan to pass it on not only to other graduate students but to every soul that needs it.

Not everyone who had an influence on my graduate school experience is a student. I thank the administrative arms of both Vanderbilt and Fisk Universities. I had very few problems and that just gave me more time to focus on the main task, so thanks to the front offices of Mechanical Engineering and Materials Science. I even want to thank the staff of WFSK for always being encouraging and especially for providing gifts of entertainment. Though I never applied, I appreciated the Bridge Program for absorbing me; because the students they accepted were definitely on a track parallel to mine, and I am glad I had their camaraderie.

For the technical acknowledgements, this research was conducted while affiliated with the Thermal Engineering Lab. Funding was provided for me by the National Science Foundation Integrative Graduate Education and Research Traineeship and the

Department of Defense (DoD) Science, Mathematics, and Research for Transformation fellowship. Computational resources were provided by the Air Force Research Laboratory DoD Supercomputing Resource Center and ACCRE at Vanderbilt.

TABLE OF CONTENTS

Page

LIST OF TABLES

Table Page

LIST OF FIGURES

Figure Page

CHAPTER I

INTRODUCTION

The rediscovery of carbon nanotubes (CNTs) by Iijima unveiled a material that offers promise in many areas of composite engineering [1]. Carbon nanotubes are shown to have exceptional mechanical, electrical, and thermal properties. Though their high room temperature thermal conductivity suggests that their inclusion in composite materials should yield a better thermally conducting composite, experimental studies have shown inconsistent thermal enhancement at best. Studies that have focused on incorporating CNTs in composites to enhanced thermal properties have studied the changes in the thermal conductivity of the matrix material—usually a polymer; few studies focus on the changes in the CNT's thermal conductivity when added to the matrix. By understanding the behavior of the individual CNT, better techniques can be developed to engineer composites with the desired properties.

Molecular dynamics (MD) simulations offer a technique to understand the atomic behavior of the CNT and between the CNT and the matrix material. Using MD simulations, thermal conductivity of the CNT can be studied to identify the contribution of individual phonon modes and how the modes are affected by interaction with the surrounding material. Insight can be obtained about how thermal conduction occurs in the CNT when incorporated into different configurations with the matrix material. This study will show that not all phonon modes contribute to increasing thermal transport, but rather their presence may actually produce more scattering.

Conduction in Bulk Materials

The nanoscale size of CNTs makes them materials that are unique from their bulk material counterpart. Often nanostructure's properties differ from those of the bulk material due to the effect of their small size. Size effects can cause a material to have "super" mechanical, electrical, chemical, or thermal properties when compared to the bulk material. This is often the result of having a larger aspect ratio, larger surface area, or small characteristic length. When considering heat transport in CNTs, a comparison to heat transport in bulk carbon materials illustrates the superior performance of the CNT.

Three mechanisms by which heat can be transferred include: conduction, convection, and radiation. Heat transfer by conduction occurs through a material due to a temperature difference, convection happens when fluid flow carries heat, and radiation carries heat by electromagnetic waves (Figure 1). Only the former process is considered

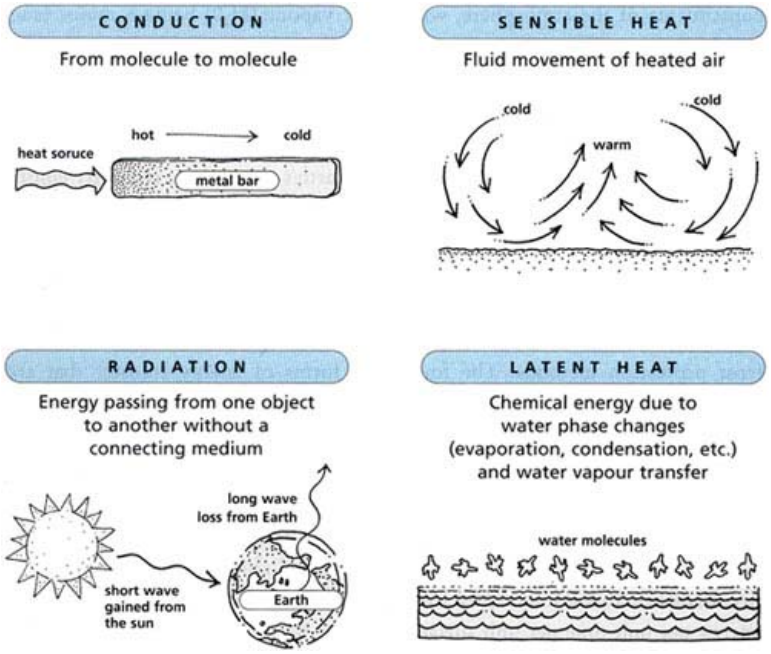

Figure 1 Methods of heat transfer **[2]**

in the scope of this work. Heat conduction occurs when thermal energy is transported by the random motion of heat carriers, which causes a temperature gradient to form in a material. The temperature gradient is the driving force that transports energy in the system; however, this is only true when the system is in a nonequilibrium steady state (Figure 2**)**. If reservoir 2 has a higher temperature than reservoir 1, then thermal energy

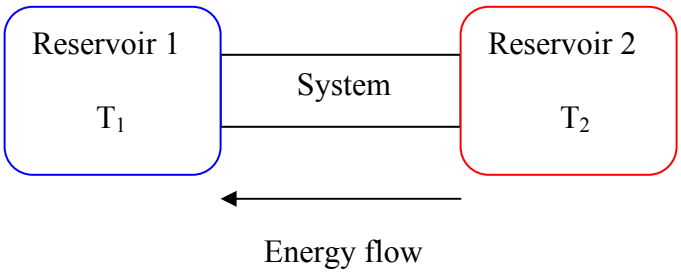

Figure 2 A nonequilibrium state exists when a system is in contact with two reservoirs of temperatures T_1 and T_2 **[3]**

will flow through the system from reservoir 2 to reservoir 1 in order to establish equilibrium; however, if the reservoirs are large their temperatures will be maintained and a temperature gradient occurs in the system. The steady state characteristic arises from the heat flux not changing with time. Heat conduction can be described by Fourier's law that states the heat flux is proportional to the temperature gradient

$$\mathbf{q} = -k\nabla T \tag{1.1}$$

where $\boldsymbol{q}$ is the local heat flux, k is thermal conductivity, ∇ is the gradient operator such that the temperature gradient is defined

$$\nabla T \equiv \frac{\partial T}{\partial x}\hat{\mathbf{x}} + \frac{\partial T}{\partial y}\hat{\mathbf{y}} + \frac{\partial T}{\partial z}\hat{\mathbf{z}} \tag{1.2}$$

where $\hat{\mathbf{x}}$, $\hat{\mathbf{y}}$, and $\hat{\mathbf{z}}$ are unit vectors [5]. The negative sign arises from the energy flowing down the temperature gradient [6]. Thermal conductivity is a material dependent

property that measures the effectiveness in conducting heat. Thermal conductivity is dependent on the direction of the material; therefore, it can be written as a tensor.

Solid materials can have thermal energy carried by phonons, as well as electrons. Phonons are atomic lattice vibrations. Depending on the material either phonons or electrons will dominate as heat carriers. For example, in metals electronic contribution is dominant at all temperatures; however, for semiconductors the mean free path (MFP) of electrons can be reduced by the presence of impurities, which allows phonons to increase their contribution to the heat current. Finally, insulators will have phonons as the dominate heat carriers [7]. Carbon materials' thermal conductivity tends to be dominated by phonons due to sp^3 and sp^2 covalent bonding, which facilitates phonon travel over the stiff bonds. Each phonon has a specific wavelength. In CNTs the wavelength of the phonon has a major influence on the amount of thermal energy transported, since the amount of energy transported increases as longer wavelengths can be included; consequently, the wavelengths can be shortened due to the presence of scattering events like defects, impurities, and functionalizing groups.

Furthermore, acoustical phonons carry the majority of heat in materials. Phonons modes can be described by polarization and branch. Typically, there are three polarizations: one longitudinal and two transverse. The number of branches depends on the number of basis atoms in the unit cell; but the branches are categorized as acoustical or optical. One acoustical branch exists for each polarization and the remaining branches are optical branches. In CNTs there exist four polarizations: three are translational and one is rotational. The translational modes are longitudinal (L), radial breathing (B), and

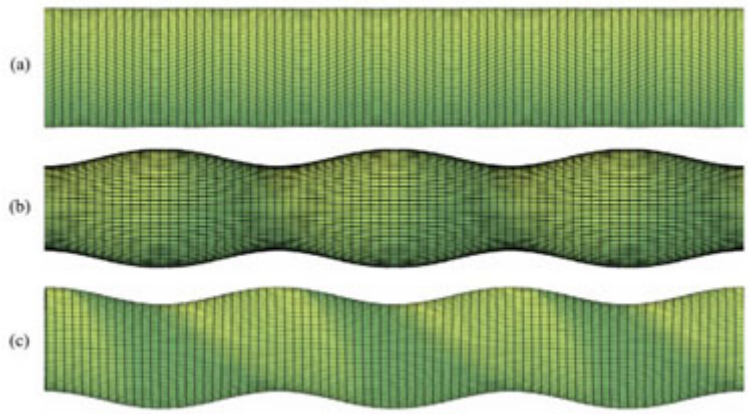

Figure 3. The translational modes in CNTs are shown (a) longitudinal, (b) radial breathing, and (c) flexural.

flexural (F). Figure 3 depicts the translational modes in a CNT. The longitudinal modes displace atoms parallel to the CNT's axis. Radial breathing modes expand and contract around the CNT's axis. Flexural modes displace atoms normal to the axis. The torsional (T) mode twists in the direction of CNT's chiral vector. Thermal energy transported in a material is the combination of energy transported by all the phonon branches for each polarization.

Thermal conductivity due to the phonons of a material can be written

$$k = \frac{1}{3} C v l \tag{1.1}$$

where C is the specific heat, v is the group velocity, and l is the phonon MFP [7]. Specific heat is a measure of the heat required to change a certain mass of the material by a specified temperature or, alternatively, the heat capacity C_v per unit mass where

$$C_v \equiv \left(\frac{\partial U}{\partial \tau} \right)_V \tag{1.2}$$

for a constant volume [3], where the fundamental temperature $\tau = k_B T$ and the internal energy U of the system can be written

$$U = \int E f(E) D(E) dE \tag{1.3}$$

where E is energy; $f(E)$ is the Bose-Einstein distribution function

$$f(E) = \frac{1}{\exp\left(\frac{E-\mu}{\tau}\right) - 1} \tag{1.4}$$

where μ is the chemical potential; and $D(E)$ is the density of states. The group velocity specifies the direction and speed at which a wave of energy propagates. The phonon MFP is the avearge distance a phonon will travel before scattering. The MFP can be written as function of the scattering time t (usually denoted τ)

$$l = t\nu\,; \tag{1.5}$$

therefore, a larger average MFP results from a larger scattering time, since scattering events occur less frequently. Scattering events can be caused by scattering due to other phonons, impurities, defects, and/or electrons [8]. In bulk carbon materials the MFP will be much smaller than the size of the material; however, the size of a CNT is comparable to the MFP. Since the MFP is a larger influence than the specific heat or group velocity, events that influence the MFP will play a larger role in the thermal conductivity. The average length of the MFP in CNTs can be decreased by the presence of functionalizing groups. Also, the interaction between phonon modes can cause the MFP to be shorter than what might be observed by with a single phonon mode.

Conduction in Nanostructures

Thermal transport can be described as diffusive or ballistic. Diffusive thermal transport occurs when phonons scatter while traveling through the system; on the other hand, ballistic transport has no internal scattering events [4]. These transport phenomena

can be related to the MFP—the average distance travelled before a scattering event occurs. When the size of the system is larger than the MFP, scattering events will occur causing diffusive transport. In ballistic transport, the MFP is larger than the system size; therefore, no scattering of the phonon can happen before the end of the system is reached. Fourier's law is based on the presence of a temperature gradient—and consequently, diffusive transport. In the case of ballistic transport, a temperature difference, rather than gradient, exists between the ends of the system [7]. When ballistic transport occurs, the only scattering event in nanostructures stems from the boundary of the system. Thermal conductivity scales with the system size; in the ballistic regime, increasing the system's size allows phonons of longer wavelengths to contribute to thermal transport and increase conductivity. If a crystal lattice is perfect, then thermal conductivity is intrinsic and limited by the anharmonicity of the interatomic forces. The intrinsic scattering processes can be normal (N) or Umklapp (U) processes. When phonons are scattered by N-processes momentum is conserved; however, U-processes do not conserve momentum and are responsible for thermal resistivity. Extrinsic thermal conductivity is limited by phonons scattering on defects in the crystal [7], [9]. The scope of this study will investigate the ballistic regime of CNTs at lengths up to 1 μm. Additionally, the effect of functionalizing atoms and bond strength on the MFP will be studied.

Carbon Nanotubes

Carbon nanotubes (CNTs) are rolled up sheets of graphite that are confined in two dimensions. If only a single layer of graphite—known as graphene—is used to construct a CNT, then it is called a single-walled CNT (SWNT); several graphene sheets rolled up

to make concentric cylinders are known as a multiwalled CNT (MWNT). A SWNT can be named according to the direction the graphene sheet is rolled. Figure 4 shows how CNTs can be rolled up from a graphene sheet and are different based on the direction. The chiral vector that defines the CNT is

$$\mathbf{c} = na_1 + ma_2 \tag{1.8}$$

where a_1 and a_2 are the basis vectors of the hexagonal graphene sheet [10]. The integers n and m are used to characterize SWNTs, which are called armchair (n,n), zig-zag (n,0), or chiral (n,m). Armchair SWNTs have electrical properties that are metallic. Zig-zag

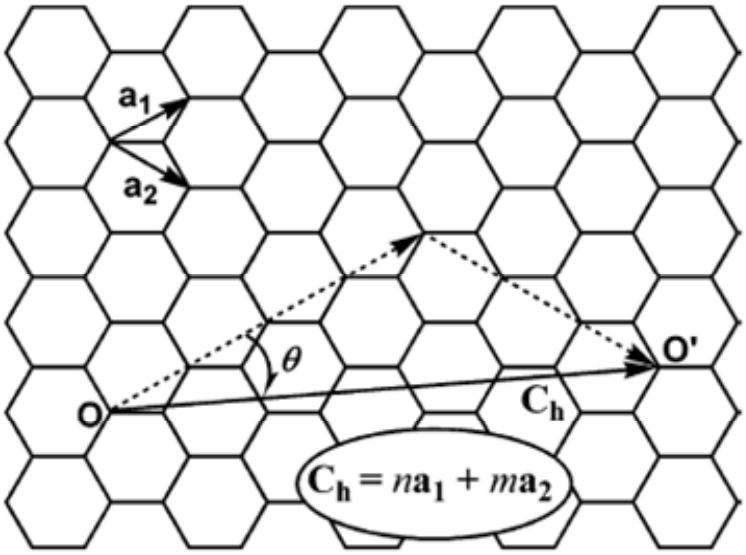

Figure 4 Starting from a graphene sheet armchair, chiral, or zig-zag CNTs can be formed based on the direction of the chiral vector **[11]**. Armchair SWNT orientation occurs when rolling the graphene sheet from left to right and zig-zag SWNT, when rolling from top to bottom; chiral SWNTs result when the sheet is rolled along any vector in between the armchair and zig-zag direction.

and chiral SWNTs are metallic if (n-m)/3; otherwise, they are semiconducting where the bandgap is inversely dependent on the diameter of the tube [11].

Like other carbon allotropes, CNTs exhibit exceptional thermal properties. The strong carbon bonds are paramount to the transport of thermal energy. The bonds between carbon atoms are strong and stiff, which is ideal for achieving high thermal conductivity. For CNTs thermal conductivity along the axis is very large. For MWNTs, thermal conductivity in the radial direction is expected to be lower; the decrease comes from the additional effect of weak van der Waals forces between the layers of the MWNT. The thermal conductivity of CNTs is generally independent of the chirality of the nanotube [12]. The length of the CNT plays a large role in the thermal conductivity in the longitudinal direction. As the length of the CNT increases, the thermal conductivity will increase as the length approaches the CNT's MFP—as the CNT becomes longer, more phonon wavelengths can participate in the thermal transport. The diameter of the CNT is related to the chirality, because larger chiralities typically lead to larger diameters; although, the larger diameter leads to increased conductance the thermal conductivity will remain independent of that fact.

CHAPTER II

LITERATURE REVIEW

Thermal Conductivity of Individual Carbon Nanotubes

Carbon nanotubes have shown a range of thermal conductivity values at room temperature (Table 1). Early experiments used samples of CNT mats, which would show a lower thermal conductivity than an individual CNT due to the interaction between the multiple CNTs [13–15]. Experiments on SWNT mats showed a thermal conductivity of 35 W/m/K at room temperature when corrected for the sample's low density [13]. Measurements of MWNT films had a thermal conductivity of 15 W/m/K; the MWNTs were estimated to have a thermal conductivity of 200 W/m/K when corrected for volume [14]. Hone *et al.* measured thermal conductivity parallel to the axis of a SWNT mat to have a thermal conductivity of ~225 W/m/K [15]. Using measurement devices that suspend the CNT, thermal conductance was measured for individual CNTs and thermal conductivity estimates were consistently shown to be well over 1000 W/m/K. Kim *et al.* determined thermal conductivity for an individual MWNT with a diameter of 14 nm was ~3000 W/m/K [16]. A thermal conductivity of ~2000 W/m/K was measured by Fujii *et al.* using a CNT with a diameter of 9.8 nm [17]. Thermal conductivity was shown to increase with decreasing diameter. Thermal conductivity for SWNT was measured as 3000 W/m/K for a 3 nm diameter by Yu *et al.* [18]. Single-walled CNTs were measured to have 3500 W/m/K by Pop *et al.* [19]. Small *et al.* measured thermal conductivity of MWNT on a microfabricted suspended device to be >3000 W/m/K [20]. When using the

Table 1 Thermal conductivities of CNT samples

Sample	Length (nm)	Measurement Method	Thermal conductivity at 300 K (W/m/K)	Reference
SWNT mat	$2x10^6$	Comparative: constantan rod	0.7 (35 corrected for density)	[13], [23]
(10,10) SWNT	1	Equilibrium MD	6600	[25]
(10,10) SWNT	<50	Equilibrium MD	2980	[26]
Magnetically aligned bulk SWNT	$5x10^3$	Comparative: constantan rod	~225	[15]
MWNT	$2.5x10^3$	Microfabricated suspended device	~3000	[16], [27]
(10,10) SWNT	15.1 - 21.1	NEMD	~1500	[12]
MWNT films	$10 - 50x10^3$	Pulsed photothermal reflectance	~15 (200 corrected for volume)	[14]
(10,10) SWNT	~400	NEMD	~300	[28]
MWNT	$2x10^6$	Microfabricated suspended device	>3000	[20]
(10,10) SWNT	<50	Homogenous nonequilbirum Green-Kubo	~2000	[29]
(5,5) SWNT	10.8	NEMD	800	[30]
Individual CNT	$3.7x10^3$	Sample-attached T-type nanosensor	>2000	[17]
SWNT	$2.76x10^3$	Microfabricated suspended device	3000	[18]
MWNT	$\sim 1x10^3$	2-point 3ω	830	[21]
(10,10) SWNT	~40	Equilibirum MD: Green-Kubo	~1635	[31]
SWNT	$2.6x10^3$	Direct self-heating	3500	[19]
MWNT	$1.4x10^3$	4-point 3ω	300	[22]

3ω method, Choi *et al.* found one MWNT sample to have 830 W/m/K [21]. Thermal conductivity of 300 W/m/K for a MWNT was measured by four-point 3ω method [22]. Using a four pad setup in the 3ω method improves the accuracy of the measurement, because contact resistance can be eliminated. The lower measurement by Choi *et al.* when using the improved technique most probably arises from the samples, since the two-point 3ω method used a MWNT with a diameter ~40 nm and the four-point 3ω method used a MWNT with a diameter ~20 nm. All the measurements have CNTs that are at least several microns long, yet thermal conductivities at room temperature are exceptionally large. This result is an indication that the phonon MFP is quite large for CNTs.

Measuring the thermal conductivity of individual CNTs has received much attention over the last decade. Initially, a comparative method using a constantan rod was used to measure bulk SWNT samples [13], [15], [23], [24]. Temperatures from 8-350 K were used by Hone *et al.* to measure SWNT mats. Later Hone *et al.* measured the thermal conductivity of aligned SWNT mats. Llaguno *et al.* measured thermal conductivity for bulk SWNTs from 10-100 K. Another technique used to measure bulk samples, the pulsed photothermal reflectance technique, was used by Yang *et al.* to measure thermal conductivity in MWNT films [14]. The development of suspended microfabricated devices has made possible measuring thermal transport in a single CNT free from substrate influence [16], [18], [19]. A microfabricated suspended heater device is used to measure thermal conductance from 8-370 K of an individual MWNT and from 100-300 K for a SWNT [16], [18], [20]. Using a sample-attached T-type nanosensor, Fujii *et al.* measured temperature dependence from 100-320 K, as well as diameter

dependence [17]. Another temperature dependent study of SWNTs employs direct self-heating for 300-800 K. Choi *et al.* used the 3ω method to measure thermal conductivity on individual MWNTs [21]. Using a four-point 3ω method, Choi *et al.* calculate thermal conductivity for an individual MWNT [22]. Length-dependent thermal conductivity was measured for an individual SWNT using a four-pad 3ω method [32].

The thermal conductivity of a CNT is estimated because only thermal conductance can be determined from an experiment or simulation. Kim *et al.* measured the thermal conductance of a MWNT and estimated a thermal conductivity of approximately 3000 W/m/K at 300 K [16]. In 2005 Yu *et al.* measured a SWNT's thermal conductance and estimated the room temperature thermal conductivity could range from 3000 W/m/K if the SWNT's diameter is 1 nm to 10000 W/m/K if the diameter is 3 nm [18]. Each of these studies measure thermal conductance rather than thermal conductivity; therefore, thermal conductivity is based on an estimation of the CNT's cross-sectional area. The area of a CNT, however, is ambiguous since its cross-sectional area is a ring with the thickness of a carbon atom. Hone *et al.* used a cross-sectional area of a tube in a bundle as 2.5 nm^2. A 1 Å thick cylinder was used by Che *et al.* [26]. A ring with thickness 3.4 Å is the van der Waals thickness [12], [28]; in contrast, Zhang and Li used a ring thickness of 1.44 Å [30]. The result of using different cross-section areas is yielding different estimates for thermal conductivity. A large cross-sectional area, such as a circle, will yield a smaller thermal conductivity than a smaller cross-sectional area estimate, like a ring. The influence on the thermal conductivity results, however, is minimal if the same cross-sectional area is used for all data considered. Needless to say when comparing thermal conductivity estimates from

multiple studies the cross-sectional area used by the investigators must be taken into consideration, since it will give an idea if the value is a high or low estimate.

The thermal conductivity of CNTs exhibits temperature dependence. At 100 K, thermal conductivities of SWNTs could be as high as 37000 W/m/K [25]. Thermal conductivity increases with increasing temperature to a peak around 300 K [17]. Pop *et al.* measured SWNTs for high temperatures (300-800 K) and found thermal conductivity decreases as temperatures rise above 300 K; they estimated a value of almost 1000 W/m/K for 800 K [19]. Similarly, each study reported the maximum thermal conductivity at room temperature after which the thermal conductivity declines. Also, each study reported similar room temperature thermal conductivities for both SWNT and MWNT; the diameters of the SWNTs were approximately 1-2 nm and the diameter for the MWNT was about 14 nm.

The thermal conductivities of CNTs can be influenced by several factors. The temperature dependence of thermal conductivity is affected by the heat capacity and phonon MFP—at low temperatures the MFP is long and thermal conductivity follows the heat capacity; but at higher temperatures, where the heat capacity becomes constant, thermal conductivity is governed by the umklapp scattering processes, which shorten the MFP and decreases thermal conductivity [25]. Specifically, the MFP is made up of the static MFP and umklapp MFP where at low temperatures the MFP equals the static MFP and as the temperature increases the umklapp MFP increases and thermal conductivity decreases [16]. The high thermal conductivity observed when measuring individual CNTs can be influenced by the lost of heat to the surroundings, which cause an overestimation of thermal conductivity [14]. Multiwalled CNTs may exhibit lower

thermal conductivities due to interaction between the tubes and, in the case of experiments, the presence of defects within the CNTs. The chirality can also cause differences in thermal conductivities of CNTs that have the same diameter. As the chirality decreases, the strain on the sigma bonds reduces the MFP of the CNT [12], [29]; however, Zhang and Li concluded thermal conductivity in CNTs is insensitive to chirality—they did not consider CNTs that were of equal radii, but different chiralities [30]. Cao *et al.* studied the affect of chirality in zigzag SWNTs—they showed that small diameters had higher conductivities and there was a peak temperature after which thermal conductivity would decrease [33], [34].

Molecular dynamics simulations have seen extensive use in the simulation of SWNTs' thermal conductivity [12], [25], [26], [31]. Simulations types include NEMD methods using heat baths, as well as equilibrium MD methods based on the Green-Kubo expression. Another simulation is the homogenous nonequilibrium Green-Kubo (HNEGK) method employed by Zhang *et al.* [29]

Similar to studies of experimental measurements of CNTs, theoretical studies have produced large thermal conductivity predictions. Using NEMD, Berber *et al.* estimated a room temperature thermal conductivity of 6600 W/m/K [25]. Che *et al.* used equilibrium MD, to estimate a thermal conductivity of 2980 W/m/K [26]. Thermal conductivity for (5,5) SWNT was estimated to be ~2250 W/m/K and ~1500 W/m/K for (10,10) SWNT by Osman and Srivstava [12]. The room temperature estimation by Maruyama averaged 300 W/m/K for (10,10) SWNTs and appeared to be independent of length [28]. The (5,5) SWNT studied reached a thermal conductivity of ~490 W/m/K at ~200nm. The simulation of Zhang *et al.* showed a (10,10) SWNT thermal conductivity

of ~2200 W/m/K [29]. Using equilibrium MD with the Green-Kubo formulation, Grujicic *et al.* estimated thermal conductivity to be ~1635 W/m/K [31]. The variations can be attributed to the use of different size simulations—with some systems containing only 400 atoms and others up to 6400 [25], [26].

Studies for length-dependent thermal conductivity have been conducted for CNTs. Many theoretical studies have shown thermal conductivity to converge at short lengths. Using lengths <50 nm, Che *et al.* show that thermal conductivity of a (10,10) SWNT converges to 2980 W/m/K [26]. Padgett and Brenner found thermal conductivity converged at <300 nm at a thermal conductivity of ~350 W/m/K [35]. Grujicic *et al.* found thermal conductivity converges for the (10,10) SWNT at a length of ~40 nm [31]. The convergence of the thermal conductivity implies that thermal transport has transitioned from purely ballistic to diffusive; however, other studies show thermal conductivity growing rapidly as length increases. For lengths up to 200 nm, Maruyama used NEMD simulations to show (5,5) SWNTs had a divergent thermal conductivity as length increases, but (10,10) SWNTs thermal conductivity was essentially non-divergent [28]. Thermal conductivity of SWNT's divergence is $\sim L^{\beta}$ as length L increases [28], [30]. The divergence of thermal conductivity with length was studied by Zhang and Li who found the divergence power parameter β decreases with an increasing CNT radius and also with increasing temperature indicating less divergence with increases scattering [30]. Maruyama speculated the limited motion of smaller radius CNTs contribute to the divergence [28]. Though length-dependent measurements of individual CNTs tends to be cumbersome, some experimental investigations have been conducted to explore the length-dependent behavior of CNTs. Yang *et al.* measured MWNT films using pulsed

photothermal reflectance and found the thermal conductivity of the films to be independent of the length of the MWNTs [14]. A length-dependent experiment was performed by Wang *et al.* using a four-pad 3ω method to measure thermal conductivity from 0.5-7 μm [32]. Thermal conductivity multiplied by the tube diameter was shown to increase with thermal conductivity before appearing to converge. The difference in the length scales between the theoretical and experimental studies suggests the short length simulations do not fully describe the thermal conductivity behavior of the CNTs.

Thermal Conductivity in Double-Wall Carbon Nanotubes

No MD simulations studies of thermal conductivity of DWNTs have been identified in the literature at this point in time. Of the DWNT MD simulations that do exist, the structural and mechanical properties of the DWNTs are the focus of the study. Saito *et al.* studied DWNTs to determine optimum geometries for various inner and outer diameters [36]. They concluded the minimum energy geometry depends on the interwall distance, a conclusion found by others as well [37]. Some MD simulations focus on the reaction of structures in the presence of other molecules [38]. Molecular dynamics simulations are used to estimate mechanical properties like Young's modulus of DWNTs [39]. An MD simulation of the length-dependent thermal conductivity of DWNTs will be a major contribution to theoretical studies of CNTs.

Thermal Conductivity of Functionalized Carbon Nanotubes

Using CNTs in composite materials to improve thermal properties have been studied in many aspects. Carbon nanotubes have a large aspect ratio and thermal

conductivity of 3000 W/m/K at 300 K. These advantageous properties make CNTs desirable filler for composite materials. Impediments to achieving the desired thermally-enhanced composite material exists due to resistance at the interface of the CNT and matrix material and the difficulty of enhancing mechanical and thermal properties simultaneously. The studies using CNTs as thermal enhancers are inconsistent in demonstrating an improved composite material (Table 2).

Table 2 Thermal conductivity of CNTs in Composite Applications

Sample	Loading	Method	RT Thermal conductivity (W/m/K)	Reference
MWNT in poly (α-olefin) oil	1 vol%	Transient hot wire	0.3765	[40]
SWNT-epoxy composite	1 wt%	Comparative: constantan rods	~0.5	[41]
Nitric acid treated MWNT in decene	1 vol%	Transient hot wire	0.1674	[42]
(5,5) SWNT	Up to 50% ^{14}C isotope impurities	NEMD	~350	[30]
(10,10) SWNT	10% functionalized with phenyl groups	NEMD	~25	[35]

Carbon nanotubes have produced enhancements to the thermal conductivity of the matrix material but not to the full potential of predicted CNT thermal conductivity. Though Choi *et al.* show a 160% enhancement in their nanotube-in-oil suspension with only 1 vol% of MWNTs added, the thermal conductivity of the oil is enhanced from 0.1448 W/m/K to 0.3765 W/m/K [40]. Acoustic impedance mismatch at the interface of the liquid and solid prevents larger enhancement [40]. The results the treated MWNTs of Xie *et al.* do not demonstrate increased enhancement, but rather produces less enhancement. Similar results are shown in composites, Biercuk *et al.* showed an increase

in thermal conductivity of the epoxy resin from ~0.2 W/m/K at 300 K to ~0.5 W/m/K [41].

Suspensions were the first systems to provide insight on thermal conductivity with CNT fillers. Choi *et al.* produced a nanotube-in-oil suspension using MWNTs and found the effective thermal conductivity of the oil increased with a small volume fraction of MWNTs [40]. They measured enhancement of the oil (160%) greater than any enhancement predicted by theoretical models of solid/liquid suspensions (10%). Suspensions of pristine and treated MWNTs in distilled water, ethylene glycol, and decene were measured by Xie *et al.* [42]. The surfaces on the MWNTs were treated with nitric acid. For the treated MWNTs, they demonstrated enhancements of 7%, 12.7%, and 19.6% for distilled water, ethylene glycol, and decene, respectively. Biercuk *et al.* measured a 125% enhancement with 1 wt% of SWNTs added to an epoxy resin. Thermal conductivity enhancement is attributed to ballistic heat conduction and to the large aspect ratio [40], [41]. When nanotubes are surface treated, thermal conductivity in suspensions is governed by matching the frequency of phonons at the interface. For instance high frequencies in the CNT must be converted to lower frequencies before energy can be exchanged with the surrounding medium [43].

The success of CNT suspensions were followed by the study of solid CNT-based composites. Several experimental studies use CNTs to thermally enhance the thermal properties of epoxy resins. Biercuk *et al.* studied the thermal enhancement of single-walled CNTs (SWNTs) in an Epon 862 epoxy resin [41]. With only 1 wt% of SWNTs, the result was a 125% enhancement relative to the pristine epoxy; however, the thermal conductivity of the composite was ~0.5 W/m/K, since the pristine epoxy's thermal

conductivity was ~0.2 W/m/K. In addition to SWNTs, Moisala *et al.* also used multiwalled CNTs (MWNTs) in their study to enhance bisphenol-A resin [44]. Use of 0.1-0.5 wt% of SWNTs reduced the thermal conductivity of the pristine resin from ~0.25 W/m/K to ~0.23 W/m/K. The MWNTs, on the other hand, increased thermal conductivity to ~0.29 W/m/K. In both studies the effective thermal conductivity is below theoretical predictions [45]. Biercuk *et al.* did not yield any conclusions on what mechanisms cause the SWNTs to yield a thermal enhancement. The only conclusion related to thermal conductivity was to mention the large aspect ratio and nanoscale diameter make SWNTs preferable over carbon fibers, because SWNTs can form an extensive network at a lower weight percent; however, this attribute is usually more applicable to electrical conductivity, rather than thermal conductivity because electrons travel along low resistance pathways whereas phonons travel through atomic vibrations. Moisala *et al.* concluded the decrease in thermal conductivity when using SWNTs was caused by either a large interface resistance due to poor phonon coupling between the SWNT and the polymer or dampening of the phonons of the SWNTs. In the case of phonon dampening, the MWNTs could sustain a higher thermal conductivity because the inner walls could continue to carry phonons. An approach to address both phonon dampening and interfacial resistance is functionalizing CNTs.

Molecular dynamics simulations were used to investigate the influence of surface anomalies on the thermal conductivity of SWNTs. Any disturbance in the CNT's topology results in a decrease in thermal conductivity. Che *et al.* completed a study on the affects of vacancies and defects on the thermal conductivity of a SWNT. Vacancies were found to cause more degradation in the thermal conductivity than defects; from the

simulations, the lowest observed thermal conductivity was 400 W/m/K for a 0.01 vacancy concentration and 1500 W/m/K for a 2.5 defect concentration. Che *et al.* concluded that defects preserve the general structure of the SWNT and bonding characteristics; however, vacancies presented no more of an influence on a one-dimensional CNT than would have been present on a three-dimensional diamond [26]. Padgett and Brenner extended the study of surface defects' influence on SWNT's thermal conductivity by adding covalently bonded phenyl rings [35]. At ~125 nm, a (10,10) SWNT with 0.25% of its atoms functionalized with phenyl groups shows a decrease in thermal conductivity of 100 W/m/K; at 10% functionalization at the same length thermal conductivity is only ~25 W/m/K [35]. Concluding, the MFP of the phonons was reduced when only 1% of the CNT's atom was functionalized and resulted in a decrease of thermal conductivity by a factor of 3. Studies have shown that thermal conductivity decreases when CNTs have impurity or functionalizing atoms included. Zhang and Li used NEMD to simulate the influence ^{14}C isotope impurity has on the thermal conductivity of (5,5) SWNTs [30]. As the percentage ^{14}C isotopes is increased in the (5,5) SWNT, thermal conductivity decreases from a maximum of 800 W/m/K when there are zero impurities to ~300 W/m/K when 50% of the carbon atoms are ^{14}C isotopes. Additionally, over all temperatures studied a 40% ^{14}C SWNT has thermal conductivity that is at most 60% of the thermal conductivity of a pristine SWNT. The impurities cause the phonon-phonon scattering that shortens the MFP of the CNT.

Functionalization of CNTs in experimental studies has shown more consistent results. Gojny *et al.* studied nanotube-based composites using SWNTs and functionalized and unfunctionalized DWNTs and MWNTs [46]. Their results indicate

thermal conductivity is dependent on phonon mechanisms, since increasing the CNT loading improves electrical conductivity—which is based on a percolation mechanism—but not thermal conductivity. Similar to Biercuk *et al.*, MWNTs outperformed SWNTs; additionally, DWNTs yielded a higher thermal conductivity as well. When the DWNTs and MWNTs are functionalized with amino groups, thermal conductivity is lower than the unfunctionalized CNTs. The conclusion is a weaker interaction between the CNT and the matrix allows the CNT to transport more efficiently because the coupling is weaker. Minimizing the coupling between the CNT and matrix reduces phonon dampening in the CNT, which reduces the CNT's thermal conductivity. Like previous studies, the composites' thermal conductivities are not largely improved over that of the pristine resin. Understanding the CNT's response to the matrix interaction is essential to engineering thermally-enhanced composites.

Thermal Conductivity in Graphene

Graphene, which is an unrolled SWNT, has been measured and found to have thermal conductivities that are larger than CNTs. Balandin *et al.* used confocal micro-Raman spectroscopy to make the first measurement of suspended single-layer graphene [47]. Similar to experiments with CNTs, the acoustic phonons are found to account for the majority of the contribution to thermal conductivity. The Klemens' approximation was used by Nika *et al.* to predict thermal conductivity in graphene flakes [48–51]. They showed that various Gruneisen parameters, a measure of the effect of changing a crystal's volume has on vibrational properties [52], influence thermal conductivity in the graphene flakes of different lengths and temperatures. The long phonon mean free path in graphene is attributed with the large thermal conductivities, since boundary scattering

dominates when the width of graphene is comparable to the mean free path. A similar result is found by Hu *et al.* while studying thermal conductivity and rectification in graphene nanoribbons [53]. Graphene nanoribbons with a zigzag chirality showed higher thermal conductivities than armchair; symmetrical and defect free graphene nanoribbons had thermal conductivities higher than the alternative. Different phonon scattering rates (and by extension mean free paths) yield the various thermal conductivities found in the different graphene nanoribbon models. Graphene nanorribon thermal conductivity was found to have sensitivity to edge shape, width, and strain by Guo *et al*. [54].

Table 3 Room Temperature Thermal Conductivity in Graphene

Sample	**Length**	**Method**	**Thermal Conductivity (W/m/K)**	**Reference**
Single layer graphene	~3 μm	Confocal micro-Raman spectroscopy	5300	[47]
Graphite monolayer	1 nm	Equilibrium MD	~6600	[25]
Single layer graphene	1-5 μm	Confocal micro-Raman spectroscopy	3080-5150	[55]
Graphene flakes	1-50 μm	Klemens approximation [48], [49]	~8500	[50], [51]
Graphene nanoribbons	~5 nm	MD	~2000	[53]
Graphene nanoribbons (armchair)	11 nm	NEMD	218	[54]

CHAPTER III

MOLECULAR DYNAMICS

Molecular dynamics (MD) simulations provide the ability to understand materials at a length scale where direct measurement is often difficult. Molecular dynamics simulations are a method of analyzing the behavior of a material at the atomistic scale. Molecular dynamics simulations are numerical computations of the estimated path of an atom or molecule. Classical MD simulations are based on Newton's second law of motion and an interatomic potential. If the mass and the interatomic potential are known, then the next position in time can be determined. Results of the calculated trajectory can be analyzed to determine properties, like thermal conductivity [4].

Newtonian Equations of Motion

The trajectory of an atom is estimated by solving Newton's second law of motion. This simple equation becomes a complex computation since each atom's equation of motion must be solved. The general Newtonian equation of motion for a system of N atoms is shown

$$\sum_{\substack{j=1 \\ j\neq i}}^{N} \mathbf{F}_{ij} = m_i \frac{d^2\mathbf{r}_i}{dt^2} \qquad i = 1,2,...,N \tag{3.1}$$

where $\boldsymbol{F}_{ij}$ is the force exerted on atom i caused by atom j and m_i and $\boldsymbol{r}_i$ are the mass and position of atom i, respectively. A limitation of the Newtonian equation is it requires additional equations to describe rotational motion [4]. By using the Lagrangian or

Hamiltonian equations of motion, all the degrees of freedom of an atom's trajectory can be obtained in one vector of generalized coordinates, **r**. The system's Lagrangian is defined as the difference of the kinetic energy and potential energy,

$$L(t,\mathbf{r},\dot{\mathbf{r}}) = K(\mathbf{r},\dot{\mathbf{r}}) - U(\mathbf{r}) \tag{3.2}$$

here $\dot{\mathbf{r}}$ is the time derivative of ***r*** or the generalized velocity. The Lagrange equation of motion is

$$\frac{d}{dt}\left(\frac{\partial L}{\partial \dot{\mathbf{r}}_i}\right) - \frac{\partial L}{\partial \mathbf{r}_i} = 0 \tag{3.3}$$

the subscript *i* denotes the generalized coordinates for each atom. Similarly, the Hamiltonian describes the energy of the system; however, it describes the total energy of the system

$$H(t,\mathbf{r},\mathbf{p}) = K(\mathbf{p}) + U(\mathbf{r}) \tag{3.4}$$

the Hamiltonian is a function of the generalized coordinate vector ***r*** and a generalized momentum ***p***. The generalized momentum is derived from the Lagrangian by differentiating with respect to the generalized velocity

$$\mathbf{p} = \frac{\partial L}{\partial \dot{\mathbf{r}}_i} \tag{3.5}$$

the Hamilton equations of motion are

$$\dot{\mathbf{p}}_i = -\frac{\partial H}{\partial \mathbf{r}_i} \qquad \dot{\mathbf{r}}_i = \frac{\partial H}{d\mathbf{p}_i} \tag{3.6}$$

Any of the three equations of motion can be used to describe the atom's trajectory.

Interatomic Potentials

The most crucial aspect of a MD simulation is the interatomic potential. The interatomic potential describes the forces that act between atoms. In order to produce reasonable results, the interatomic potential must give an accurate description of the interaction in the system. The potentials, however, are limited to being only as good as the data (either from experiments or *ab initio* simulations) upon which they are based. Molecular dynamics simulations of atoms have potentials that can be categorized as pair, many-body, and force fields. The simplest interatomic potential is one describing the interaction between two atoms—this type of potential is known as a pair potential. Examples of pair potentials include Coulomb's, Newton's law of universal gravitation, Lennard-Jones, and Morse potentials; the former two are outside the scope of this work. The Lennard-Jones and Morse potentials are often used in MD simulations.

The Lennard-Jones potential is used in MD simulations to describe non-bonded interactions. The Lennard-Jones potential is defined

$$U_{ij} = \frac{B}{r_{ij}^{12}} - \frac{A}{r_{ij}^{6}} \tag{3.7}$$

where r_{ij} is the distance between two atoms i and j, $A = 4\varepsilon\sigma^6$, and $B = 4\varepsilon\sigma^{12}$ [7], [4]. On the right-hand side, the first term is a repulsive potential, which acts when the two atoms' nuclei or inner-shell electrons begin overlapping [4]; the second term is an attractive potential caused by dipole moments that the atoms induce in one another [7]. The Lennard-Jones potential is useful for describing the interaction of crystals of noble gases, like argon. In noble gases the interactions are non-bonded, since the outer shells are completely filled. The forces between the atoms are governed by van der Waals forces. These are same forces that occur between layers of graphite and the walls of

CNTs.; therefore, the Lennard-Jones potential is useful in describing the interaction between the walls of DWNTs and between functionalizing united atoms groups and the CNT's exterior, because these are non-bonded interactions. The Lennard-Jones potential, however, is insufficient to describe the interactions associated with covalent bonds.

In the scope of this work, interatomic potentials that consider the how the interactions between two atoms are influenced by other atoms are many-body potentials and forcefields. With carbon systems like graphite, diamond, and nanotubes, the interaction between two carbon atoms depends not only on the distance between the atoms, but also on the atoms surrounding the pair. Several potentials exist that describe the interaction in carbon systems [56]; however, these potentials are largely based on mechanical properties such as Young's modulus, rather than thermal properties. Two many-body potentials that describe the covalent bonding present with structures containing carbon are the Tersoff potential and the reactive empirical bond-order (REBO) potential. The Tersoff potential is the first potential that considered bond-order and allowed for bonds to be formed and broken during the simulation, which is useful in studying chemical reactions, and it considers the bond angle between atoms i, j, and k [57], [58]. The form of the Tersoff potential gives the total energy of the system, E,

$$E = \sum_i E_i = \frac{1}{2} V_{ij} \tag{3.8}$$

where E_i is the site energy and V_{ij} is the bond energy defined as

$$V_{ij} = f_C(r_{ij})[a_{ij} f_R(r_{ij}) + b_{ij} f_A(r_{ij})] \tag{3.9}$$

the functions f_C, f_R, and f_A represent a smooth cutoff, repulsive pair potential, and an attractive pair potential, respectively; the function a_{ij} consists of range-limiting terms and b_{ij} is a measure of the bond order [58]. The REBO potential is a type of Tersoff potential

that is especially good at modeling the interactions in hydrocarbons and graphite [59]; however, the REBO potential is only good for short interactions that are intramolecular. The REBO potential was extended to include Lennard-Jones terms to account for intermolecular interactions, as well as torsional interactions [57]. The potential is called adaptive intermolecular REBO (AIREBO) potential, which is defined

$$E = E^{REBO} + E^{LJ} + E^{tors} \tag{3.10}$$

where,

$$E^{REBO} = V_{ij}^{R}(r_{ij}) + b_{ij}V_{ij}^{A}(r_{ij}) \tag{3.11}$$

the first term on the right-hand side is the repulsive pair potential and the second, attractive; the torsional term of Eqn. (2.10) defines the dihedral angle determined by atoms i, j, k, and l

$$E_{ijkl}^{tors} = w_{ki}(r_{ki})w_{ij}(r_{ij})w_{jl}(r_{jl})V^{tors}(\omega_{ijkl}) \tag{3.12}$$

where

$$V^{tors}(\omega_{kijl}) = \frac{256}{405}\varepsilon_{kijl}\cos^{10}(\omega_{kijl}/2) - \frac{1}{10}\varepsilon_{kijl} \tag{3.13}$$

The covalent bonds of CNTs use the Tersoff potential and Lennard-Jones potentials model the van der Waals forces between the layers of DWNTs and the united atom models. To study transport properties interatomic potentials that contain anahrmonicities are needed, thermal conductivity cannot be studied using a harmonic potential because scattering will not occur.

Molecular Dynamics Simulation Methods

Thermal transport properties can be determined by using MD simulations. Two simulation methods exist for using MD simulations to find thermal information—nonequilibrium and equilibrium dynamics. A nonequilibrium MD simulation method (NEMD) can be used to understand thermal transport processes; however, when using an equilibrium MD (EMD) simulation method only thermal properties can be determined. A NEMD simulation is typically faster than an EMD simulation, since the EMD simulation relies on calculation of a computationally expensive autocorrelation function; however, NEMD simulations can have inconsistencies when defining local thermal equilibrium, temperature distributions, and boundary conditions in systems with long mean free paths [4].

Two methods are popular for imposing nonequilibrium conditions on a system. One method is to impose a temperature gradient and calculate the heat flux—the other imposes a heat flux and calculates the temperature gradient sometimes called a reverse NEMD (RNEMD) simulation. Using reservoirs to control the temperature requires a large temperature difference, but by using the constant heat flux method this issue can be circumvented [4]. One implementation of a RNEMD simulation is to add and subtract a heat flux from defined hot and cold regions of the system, respectively. The heat flux is added (or subtracted) by rescaling the velocity in that region. By adding and subtracting heat fluxes in the hot and cold regions equally, a temperature gradient is established in the system. Another RNEMD simulation method introduced by Muller-Plathe, imposes a constant heat flux by exchanging kinetic energy between the hot and cold regions [60], [61]. The velocity vector of the hottest atom in the cold region is exchanged with that of

the coldest atom in the hot region—the atoms must be of the same mass to conserve linear momentum. The heat flux is known from the amount of kinetic energy exchanged during the simulation time of the system; what results for the exchange of energy is a temperature gradient between the hot and cold regions.

Alternative to the nonequilibrium methods of MD are equilibrium methods. There is no temperature difference applied to the system in EMD simulation, but rather the history of the atoms' movement in the system is used to determine thermal properties. The Green-Kubo formula can be used to find thermal conductivity directly

$$k(T) = \frac{1}{3Vk_B T^2} \int_0^\infty \left\langle \mathbf{J}_Q(t) \bullet \mathbf{J}_Q(0) \right\rangle dt \tag{3.14}$$

where V is the volume of the system, k_B is the Boltzmann constant, and $\mathbf{J}_Q$ is the heat current [4]. The term in the integral is the heat current autocorrelation function, which is a time-delayed comparison of the heat current to itself. The EMD simulation tend to be more computationally expensive than NEMD simulation methods, since the heat current must be calculated for a many time steps for all the atoms. Since length-dependent thermal conductivity experiments will be performed, the use of EMD simulations is a less desirable method than the NEMD simulation methods.

CHAPTER IV

SIMULATION METHODS

Molecular dynamics (MD) simulations of CNTs are performed to predict how thermal transport is affected by non-bonded interactions. Types of CNTs studied include single-wall CNTs (SWNTs), double-wall CNTs (DWNTs), and functionalized SWNTs and DWNTs. Using the Tersoff and Lennard-Jones potentials, simulations are performed using the Large-scale Atomic/Molecular Massively Parallel Simulator (LAMMPS) distributed by Sandia National Labs [62]. Nonequilibrium MD (NEMD) and wave packet simulations are used to gather thermal conductivity and thermal transport data.

Models of Carbon Nanotubes

Carbon nanotube coordinates used in the simulation are generated using TubeGen. TubeGen is able to produce a variety of molecular nanotubes; TubeGen has the flexibility to generate the coordinates of not only carbon nanotubes, but also other molecules like boron nitride [63]. Based on the desired chirality, TubeGen yields a tubular unit cell. Nanotubes with large chiral vectors have unit cells containing more atoms and larger diameters. To achieve a CNT of the desired length, the unit cell is replicated along the axial direction (*z*-axis); the correct number of unit cells to replicate can be obtained by dividing the length of the CNT by the length of the unit cell (~ 0.1 nm). Table 4 shows the chiralites investigated and their properties; the lengths are studied for a range of 25 nm to 4 μm.

Table 4 Characteristics of CNTs studied.

Chirality	Diameter (nm)	Atoms in Unit Cell
(5,5)	0.7	20
(10,10)	1.4	40
(19,10)	2.0	868
(37,37)	5.0	148
(80,80)	10.9	320

When using TubeGen it is important to set ample gutter spacing to obtain the correct atom coordinates; otherwise, atoms that are outside of the limits set by the gutter will be reflected back inside the box resulting not in a tube, but rather disconnected arcs (Figure 5).

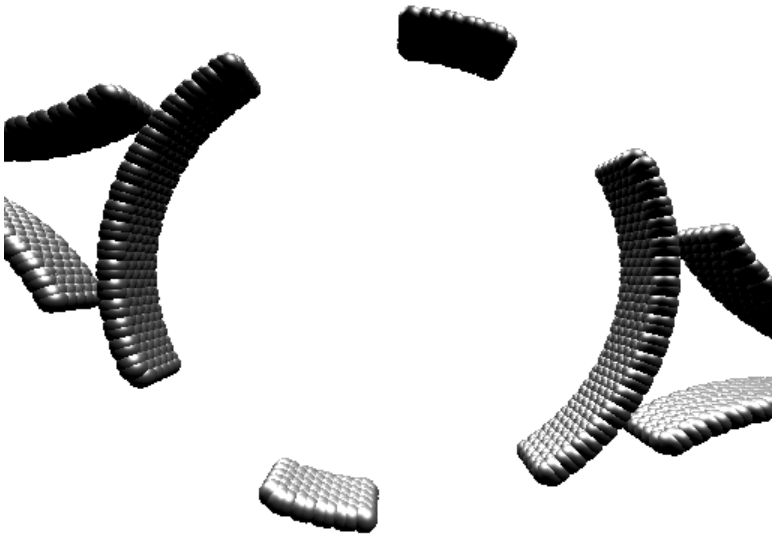

Figure 5 An example of a disconnected CNT generated by TubeGen when the gutter size is not adequate.

The TubeGen coordinate file is in *.xyz* format, which cannot be used directly by LAMMPS. An example TubeGen input script and partial output file can be found in Appendix A along with the LAMMPS formatted coordinates. An example of a typical SWNT generated by TubeGen is shown in Figure 6.

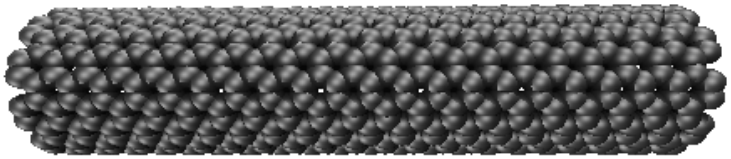

Figure 6 A chirality (10,10) CNT generated by the TubeGen coordinate generator.

From the initial SWNTs more complex models can be made. To create DWNTs, SWNTs are generated and then merged together (Figure 7). The chiralities that yields the

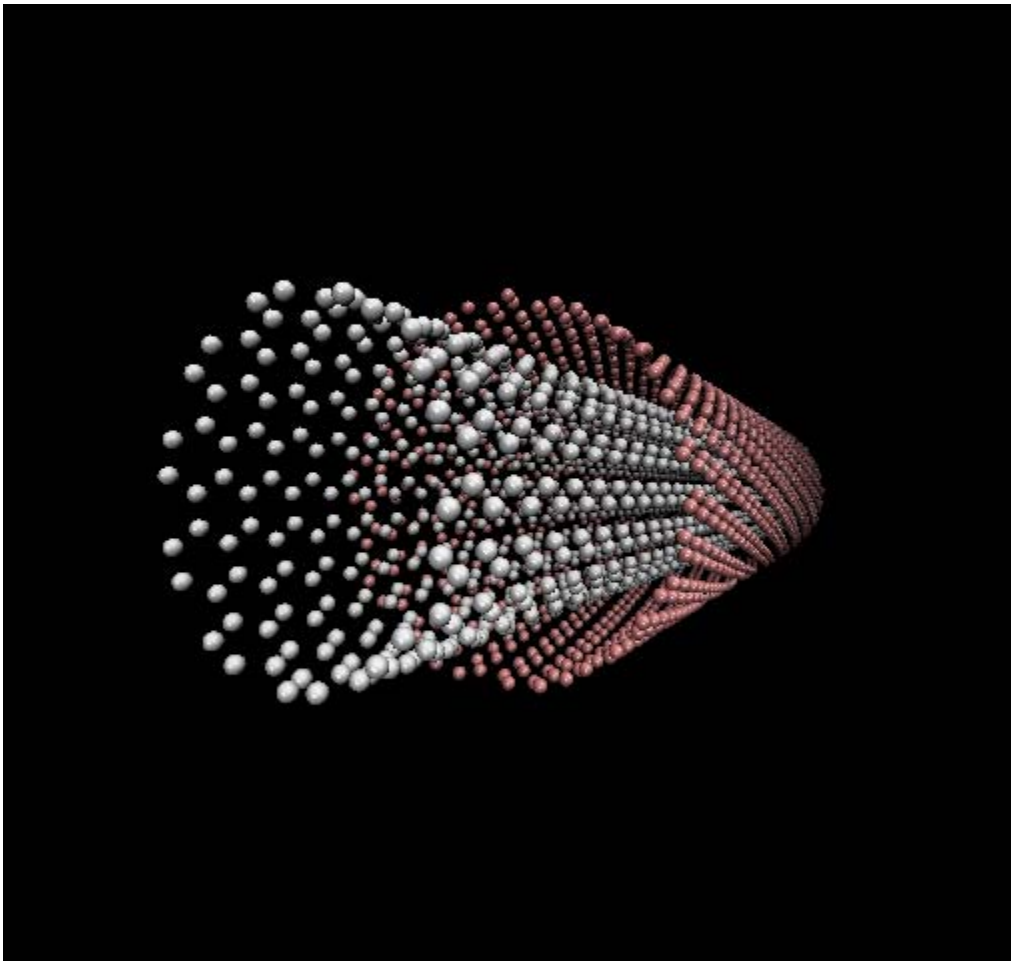

Figure 7 A typical (10,10)@(19,10) DWNT.

lowest energy DWNT is based on the diameter of the inner SWNT [37]; therefore, DWNTs with (10,10) and (19,10) SWNTs are utilized. The interwall spacing of the DWNT is about 0.6 nm. To differentiate the walls for LAMMPS, different atom types

are assigned to each SWNT; the DWNT then behaves with the appropriate interatomic interactions, which are discussed later. This same procedure can be used to specify the atoms of the functionalized CNT model; where each new element is assigned an atom type number and the interatomic potentials are determined by the atom type. The functionalized CNTs are functionalized randomly as a percentage of the number of atoms in the CNT (Table 5). The functionalizing atoms are united atom models of a phenyl group.

Table 5 Number of Functionalization Atoms for CNTs

Percentage	200 nm SWNT	200 nm DWNT
0.25%	81	120
1%	324	470
5%	1624	2352
10%	3248	4704

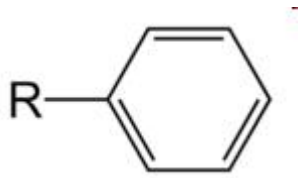

Figure 8 A phenyl group.

During the simulation, the interactions of the atoms in the simulation are governed by the interatomic potentials. Choosing the appropriate potentials is of the utmost importance because the accuracy of the results is dependent upon them. In the simulation of CNTs, the interatomic potentials that have been used are the Tersoff-Brenner potential [26], [35]; both describe the covalent bond of C atoms. The Lennard-Jones potential is used to describe the van der Waals interaction between the walls of the DWNT and between the CNT and functionalizing groups, using values of 3.345 Å and 37 K (4.8 meV) for σ and ε, respectively [64].

Nonequilibrium Molecular Dynamics Simulation Parameters

At the beginning MD simulation, the CNT must be brought to an equilibrium state. The coordinates given by TubeGen have the C atoms near their minimum energy position. Energy minimization is performed in LAMMPS using the conjugate gradient method. The velocity of the CNT is set such that the starting temperature is 300 K. Since all the energy is potential at the start, a NVE integrator in LAMMPS is used to relax the CNT, the total energy of the system comes to equilibrium in 200 ps. Using a SWNT, a 1 fs time step is sufficient and the data can be sampled every 2000 time steps without losing information. Periodic boundary conditions are applied in all directions.

Nonequilibrium MD methods can be implemented in LAMMPS through the use of *fix* commands. The Muller-Plathe method is invoked by using *fix thermal/conductivity* to swap the kinetic energy in a group of atoms; *fix heat* applies a constant flux by rescaling the velocity of a group of atoms in specified time increments. In both NEMD methods, the outputs result in the direct calculation of thermal conductance, rather than thermal conductivity; as mentioned previously, the cross-sectional area of a CNT is quite ambiguous. An estimation of area for thermal conductivity is $A=2\pi r\Delta r$; this estimate eliminates the hollow center of the CNT, which does not conduct, and incorporates Δr, an interwall spacing of 0.6 nm as a thickness of the ring.

Muller-Plathe Method

Thermal transport is simulated using a Muller-Plathe NEMD method. The CNT is divided into 20 sections in the axial direction (z-axis); the end section is cold and the

middle section is hot. Figure 9 is representative of the simulation's setup. The velocity of the atoms in one unit cell are exchanged every 15 fs for 1 ns; for example, the unit cell of a (10,10) CNT has 40 atoms. The total kinetic energy swapped is recorded and a

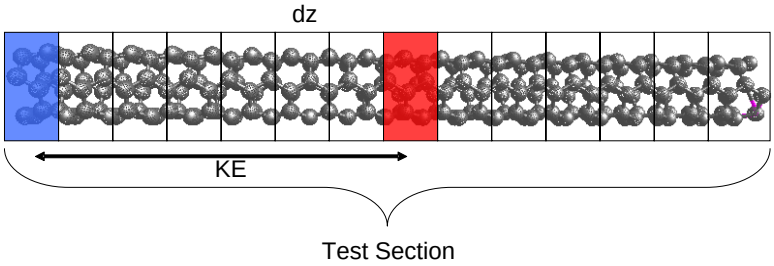

Figure 9 A representation of the setup for Muller-Plathe NEMD method in LAMMPS.

running average of the temperature in each section is calculated every 2.5 ps to find the temperature gradient. Figure 10 shows a typical temperature profile that results from the Muller-Plathe method—it is V-shaped, since the hot section is in the middle of the system. The discontinuity at the edge is due to the periodicity.

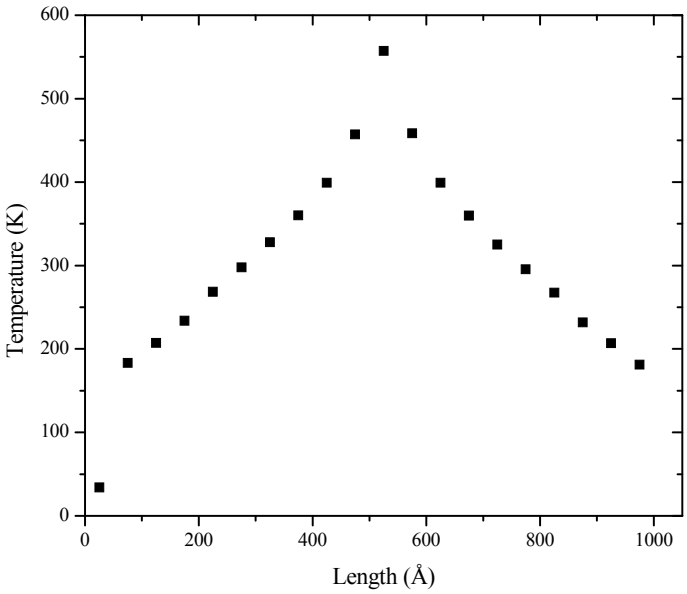

Figure 10 A typical temperature profile generated by the Muller-Plathe NEMD method.

Using the outputs from the Muller-Plathe method, the thermal conductance can be calculated using Fourier's Law in the form

$$kA = \frac{KE_{swapped}}{2t_{swap}} \cdot \frac{\Delta T}{\Delta x} \tag{4.1}$$

where k is the thermal conductivity, A is the cross-sectional area, and t_{swap} is the total time the kinetic energy swap is performed. One-half of the swapped kinetic energy is used because the heat can flow in two directions.

Heat Bath Method

Thermal transport is simulated using a constant energy flux NEMD method where the carbon nanotube is in contact with two external baths. A temperature difference between the baths is achieved by subtracting and adding a constant energy rate of 10 eV/ps every time step to the baths for 5 ns. To prevent the evaporation of any C atoms, stationary walls are placed at the ends of the CNT/bath system—Figure 11 represents the simulation's setup, which includes dividing the CNT into 20 sections in the longitudinal direction (z-axis).

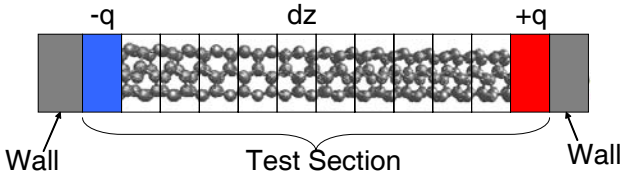

Figure 11 A representation of the setup for constant energy flux NEMD method in LAMMPS.

A running average of the temperature in each region is calculated every 2.5 ps to find the temperature difference, which is represented in Figure 12.

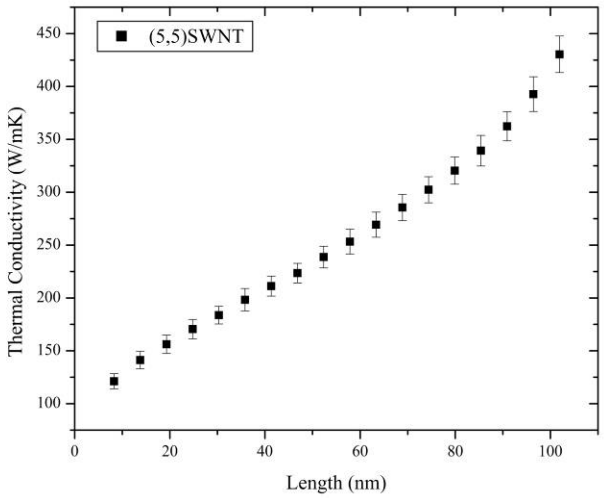

Figure 12 A typical temperature profile generated by the constant energy flux NEMD method.

From the outputs generated by the constant flux method, Fourier's law takes the following form

$$kA = q\frac{\Delta T}{\Delta x} \tag{4.2}$$

where q is the energy rate. The error of the temperature gradient in both methods is calculated from the fluctuations of the temperature in the averaged bins over the time of the NEMD simulation.

Additionally for DWNTs, two alternative simulation setups were used. One setup allows only one wall to have a temperature gradient applied and the other holds one wall stationary.

Validation

The simulation setup for the Muller-Plathe NEMD method is compared to Padgett and Brenner [35] to validate the results of LAMMPS. In their study of the influence of

chemisorption, Padgett and Brenner used the Muller-Plathe method to the find the thermal conductivity of a (10,10) SWNT as a function of length. Using LAMMPS the simulation was run with their parameters. The chosen interatomic potential was Tersoff and a time step of 0.25 fs was used. The system was equilibrated at 300 K for 2.5 ps. The Muller-Plathe method was run for at least 100 ps while swapping the kinetic energy of 20 atoms every 15 fs. Data is collected and averaged over every 2.5 ps.; the area used for the SWNT's cross-section was a 3.4 Å thick ring. The comparison of LAMMPS and Padgett and Brenner is shown in Figure 13. The results from LAMMPS show the same trends as Padgett and Brenner's results—which appear to be approaching a thermal conductivity limit as the length increases. The divergence of the LAMMPS results from Padgett and Brenner can be attributed to the SWNT needing a longer time to equilibrate where the LAMMPS results are equilibrated for 200 ps, which is an order of magnitude larger than Padgett and Brenner. The LAMMPS results are comparable to Padgett and Brenner's data, thus it is valid as a simulator for CNTs.

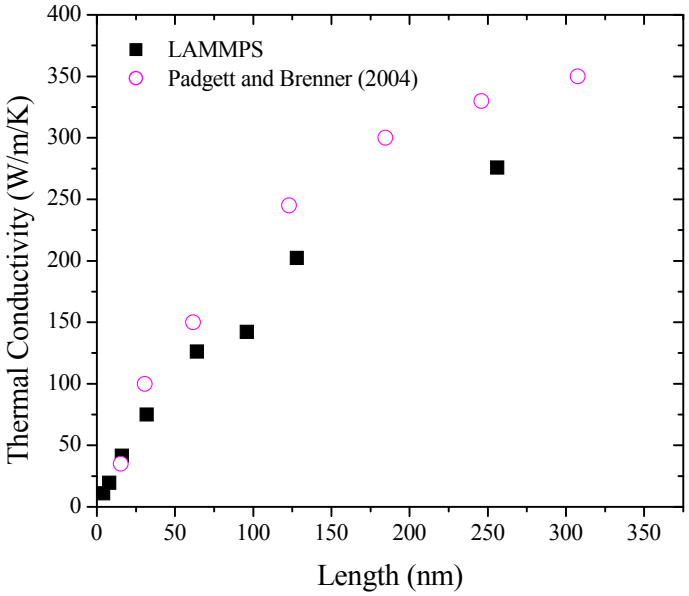

Figure 13 Comparison of thermal conductivity versus length results for a (10,10) SWNT by the LAMMPS simulator to Padgett and Brenner's 2004 study.

CHAPTER V

RESULTS AND DISCUSSION

Carbon nanotube thermal conductivity

Simulations were performed for SWNTs and DWNTs at various lengths from 25 nm-1μm. At 25 nm thermal conductivity for all CNTs studied is ~150 W/m/K; at 1 μm thermal conductivity ranges from ~1000 W/m/K for the DWNT to >1200 W/m/K for the (10,10) SWNT (Figure 14). The results presented in Figure 14 show agreement with the (10,10) SWNT results of Padgett and Brenner [35] (Figure 13). Both results are less than the values of other computational studies for similar lengths due to the use of the Tersoff potential [12], [26], [28]. The Tersoff potential overestimates anharmonicities in the potential and leads to an underestimation of thermal conductivity by ~1000 W/m/K when compared to experimental measurements [16], [18], [19], [65], [66]. Also the assumption of the cross-sectional area yields differences in the estimation of thermal conductivity as mentioned previously. Nevertheless a trend similar to studies of MWNTs and SWNTs with small diameters is shown [16], [18], [19], since comparable thermal conductivities are calculated for SWNTs and DWNTs. Unlike previous studies, thermal conductivities calculated for this study do not converge to a single value, but rather show a general increasing trend. The increase implies that longer lengths introduce phonon modes of longer wavelengths that have a significant contribution to thermal conductivity.

Plotting the thermal conductivity versus length on a log-log scale is shown in Figure 15. Similar to other studies, thermal conductivity in SWNTs is shown to diverge with increasing length [28], [30]. In 1D model calculations thermal conductivity, λ =

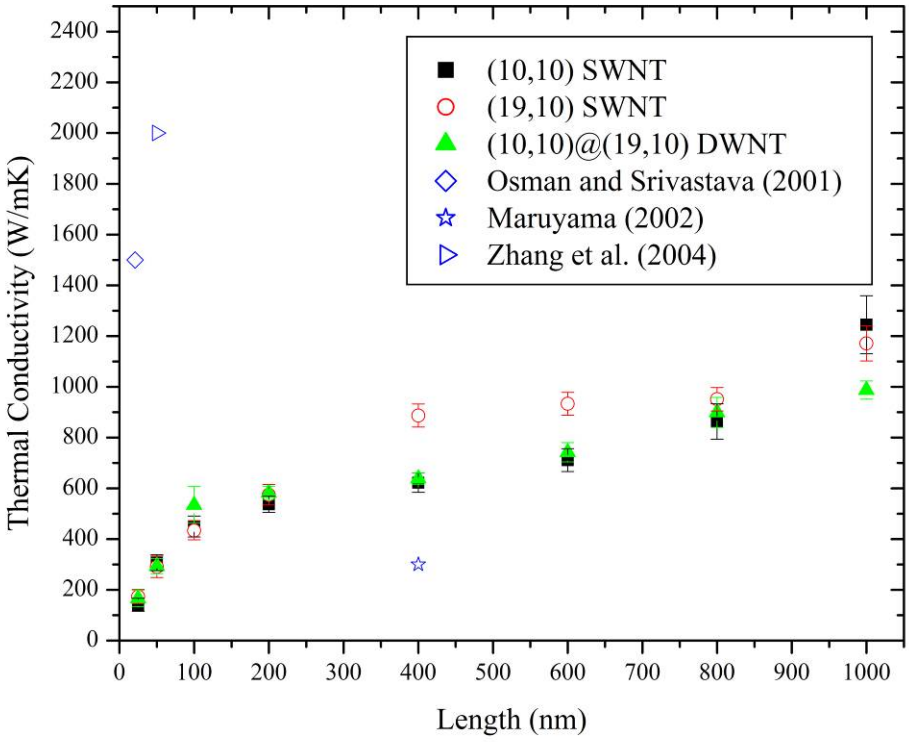

Figure 14 Thermal conductivity of (10,10) and (19,10) SWNTs and a (10,10)@(19,10) DWWNT for lengths from 25 nm to 1 μm. Also shown are the NEMD thermal conductivity of (10,10) SWNTs from other works **[12], [28], [29]**.

aL^{β}, and β values are ~0.4. When fitting the value of β, trends of the results are in agreement with previous works where β increases as the diameter decreases. For the (10,10) and (19,10) SWNTs β=0.53 and 0.43, respectively. The thermal conductivity of the SWNT, however, will eventually converge when the tube length is longer than the MFP. Maruyama *et al.* speculated that the divergence can be attributed not only to the small length of SWNTs used, but also to the limited freedom of motion caused by the smaller diameter of the (5,5) SWNT compared to the (10,10) SWNT [28]; this hypothesis appears to be supported by Zhang and Li, who show a larger β at 300 K than at 800 K, since the higher temperature is an indication of more energy and therefore more motion in the CNT [30]. Another interpretation is that β is larger when phonon MFPs are longer.

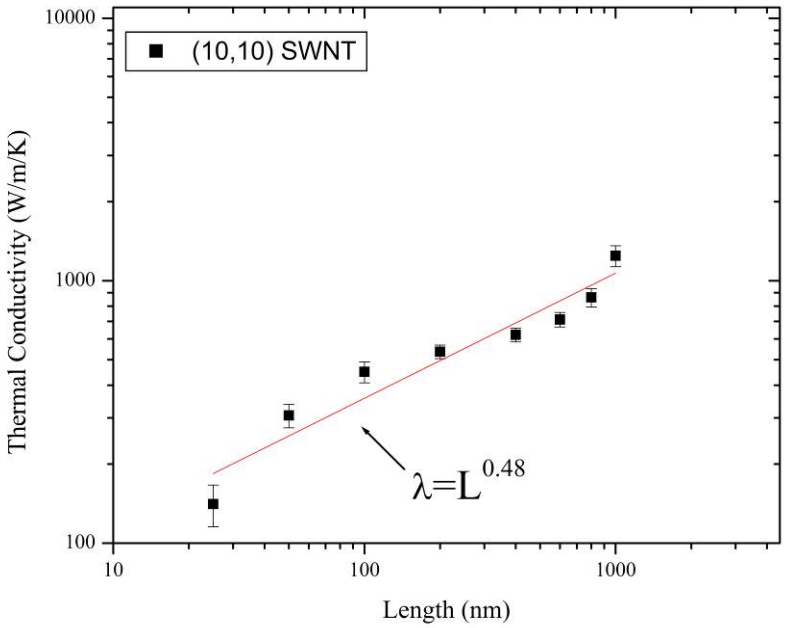

(a)

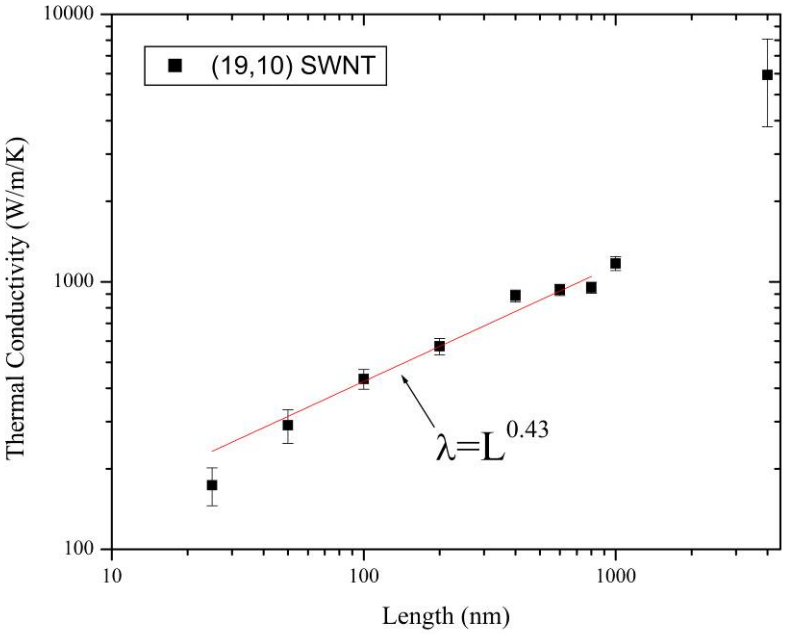

(b)

Figure 15 Thermal conductivity versus length plotted on a log-log scale for a (a) (10,10) SWNT and (b) (19,10) SWNT. The line is thermal conductivity $\lambda \sim L^{\beta}$.

When SWNTs of different chiralities are compared, the average phonon MFP can be speculated to be longer in the smaller diameter SWNT, since the radial breathing modes will be smaller and result in fewer phonon-phonon interactions with longer wavelength phonon modes.

Subsequently, simulations were performed to limit the freedom of motion in the CNTs. Double-walled CNTs are modeled that have only one wall heated or only one wall moving, which is a unique method for isolating a particular vibrational motion and identifying the contribution of that motion to the thermal conductivity of a CNT. Figure 16 shows the variation of thermal conductivity in DWNTs when the heating scheme is manipulated. When a single wall is heated and both walls are allowed to move, thermal conductivity does not deviate largely from the thermal conductivity of the DWNT in the original setup. The suggestion is van der Waals forces are strong enough to cause the unheated wall to move in sync with the heated wall; however, the forces are too weak to cause significant scattering between the walls. Consequently, when one of the walls is held stationary, the motion of the other wall is significantly restricted because of the van der Waals forces. The thermal conductivity increases by ~50% in these alternative cases where one wall is stationary. This result agrees with the trend observed with carbon peapods [67], which showed thermal conductivities that were twice as large as a pristine SWNT. Carbon peapods are SWNTs that have fullerenes on the inside. Two mechanisms of energy transfer were attributed with the increased thermal conductivity: a low-frequency radial vibration coupling between the CNT and the fullerenes and collisions between fullerenes along the axis. Some phonon mode interactions contribute more to scattering than to thermal transport. Removing or restricting these phonon

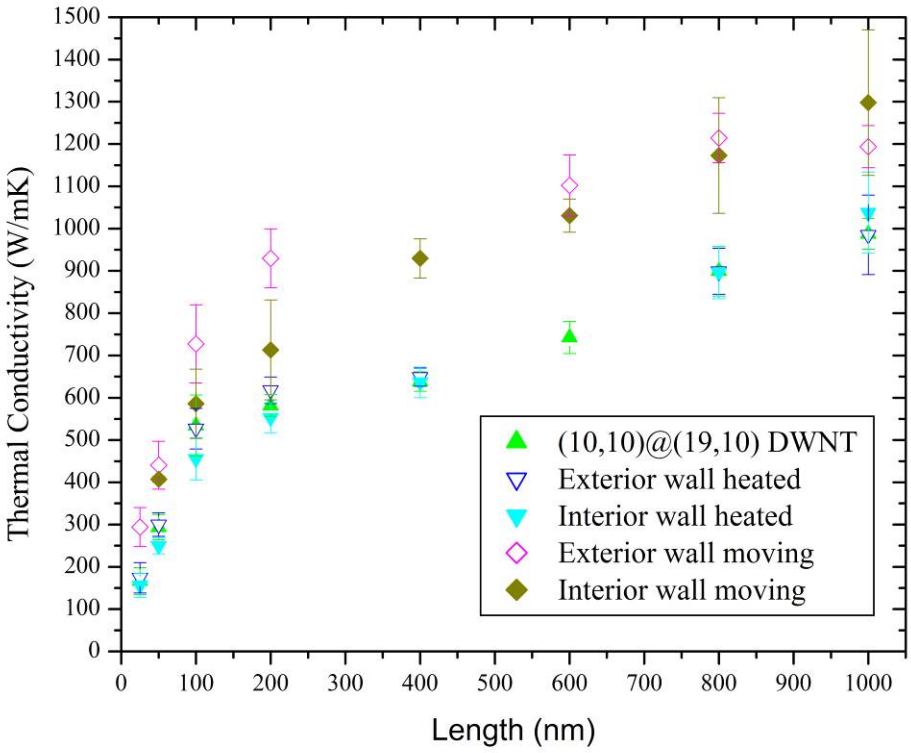

Figure 16 Thermal conductivity of DWNT using various heating schemes. Both walls are moving for the data represented by upside down triangles, but only the exterior wall is heated for the unfilled triangles and only the interior wall for the filled triangles. In contrast, the diamonds have only one wall moving: only the exterior wall for the unfilled diamonds and the interior wall only for the filled diamonds.

interactions yield a higher thermal conductivity even though fewer phonon modes are left to contribute to thermal conductivity. When either the interior or exterior wall is held stationary, the DWNT behaves as a SWNT with restricted motion. A stationary interior wall restricts flexural modes. Not only flexural modes, but also radial breathing modes are restricted when the exterior wall is stationary. Longitudinal modes are restricted by not allowing the LAMMPS' NVE integrator to update coordinates along the z-axis. This method is not an entirely perfect way of restricting modes, since the radial breathing and torsional modes also incorporate longitudinal motion, as well; however, the method yields a low estimation of a modes' contribution. Computing the mean square vibrational

amplitudes of atomic motions verifies that vibrational motion is restricted. The Cartesian coordinates of 25 nm CNTs are converted into cylindrical coordinates for the calculation. The mean square vibrational amplitude is defined

$$\left\langle u_{\alpha}^{2} \right\rangle = \frac{1}{2} \sum_{i=1}^{N} \left[\left\langle r_{i\alpha}^{2} \right\rangle - \left\langle r_{i\alpha} \right\rangle^{2} \right] \tag{5.1}$$

where α denotes radial (ρ), azimuthal (θ), axial (z) directons and the brackets <…> indicate a time average. Table 6 lists the amplitudes for CNTs with different vibrational mode restrictions. When none of the vibrational modes are restricted the mean-square vibrational amplitudes in the azimuthal direction is comparable for the SWNT and DWNT, as well as for the individual walls of the DWNT. This result is expected since the thermal conductivities are shown to be comparable. The radial and axial directions of the SWNT and DWNT show differences, which can be attributed to the DWNT having more vibrations caused by the interaction betweens the walls. The individual walls of the DWNT, however, show comparable amplitudes. This result is also an indication that the walls of the DWNT move in sync. In contrast, when all modes except the torsional mode are restricted the mean-square vibrational amplitudes in the radial and axial directions decrease by nearly and order of magnitude; meanwhile, the mean-square vibrational amplitude in the azimuthal direction remains the dominant vibrational direction. Also, when the flexural mode is present the mean-square vibrational amplitudes are larger in every direction compared to when the flexural mode is restricted. The flexural mode, therefore, carries a lot of energy. If the net change in the mean-square vibrational amplitudes is considered, then the presence of the flexural mode accounts for >80% of the amplitude increase.

Table 6. Mean-square Vibrational amplitudes for 25 nm CNTs with Various Combinations of Vibrational Modes [Longitudinal (L), Radial breathing (B), Torsional (T), and/or Flexural (F)]

	Vibrational Modes Present	$\langle u_r^2 \rangle$ (A^2)	$\langle u_\theta^2 \rangle$ (rad^2)	$\langle u_z^2 \rangle$ (A^2)
(10,10)SWNT	L-B-T-F	0.060109	0.15209	0.0014643
DWNT	L-B-T-F	0.85755	0.093327	0.026269
Interior DWNT wall	L-B-T-F	1.0662	0.097365	0.0286
Exterior DWNT wall	L-B-T-F	0.94116	0.10889	0.031191
Exterior wall motion only	L-B-T	0.0011489	0.0022555	1.8541e-4
(10,10) SWNT w/no long.	B-T-F	0.084366	0.14035	0.0017899
Interior wall motion only	L-T	0.0010928	0.044124	2.6239e-4
Exterior motion only w/no long.	B-T	0.0013686	0.0030953	2.3844e-4
Interior motion only w/no long.	T	0.0012941	0.0431	2.1897e-4

The variation of CNT thermal conductivity from different combinations of phonon modes is presented in Figure 17. As shown, thermal conductivity in SWNTs is largely affected by the longitudinal and flexural modes. Thermal conductivity is less than the unrestricted DWNT when either the torsional mode or the torsional-radial breathing mode combination is considered. The torsional mode has a smaller thermal conductivity, because it is the only mode contributing. This result can be expected since in the Holland[68] and Callaway[69] models of lattice thermal conductivity the thermal conductivity is a sum of the thermal conductivity contributed by each phonon mode. In which case, the radial breathing mode is considered to not have an appreciable influence on thermal conductivity, since its inclusion with the torsional mode results in a thermal conductivity that is comparable to the torsional mode alone. This result cannot be wholly contributed to the lack of the longitudinal motion within the breathing and torsional modes, because thermal conductivity for the longitudinal and torsional mode combination is comparable to the thermal conductivity of the longitudinal, torsional, and breathing mode combination. When the flexural mode is added to the torsional and radial breathing

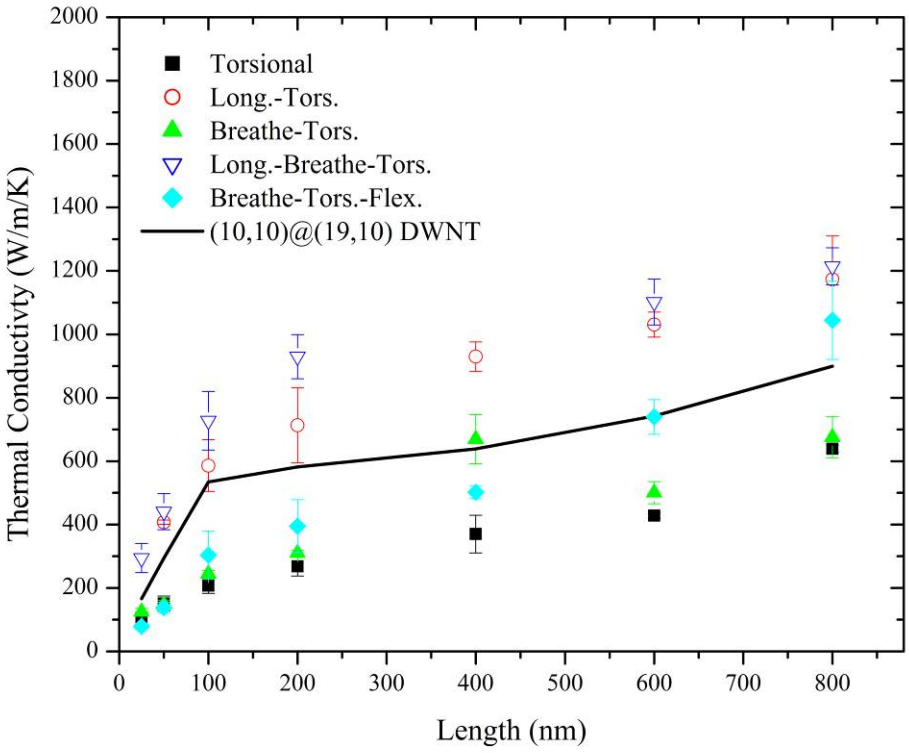

Figure 17 Thermal conductivity is shown for the CNT when combinations of modes are restricted **[70]**.

modes, thermal conductivity increases are directly proportional to length; at 800 nm thermal conductivity exceeds the unrestricted DWNT. The flexural mode can contribute more states to the thermal conductivity as the length of the CNT increases. Likewise, as the length increases the longitudinal mode in combination with torsional and breathing modes has a thermal conductivity that is greater than the DWNT, because the increased length adds additional longitudinal mode states that can contribute to thermal conductivity. However, the combination of the longitudinal and flexural modes in CNTs result in a thermal conductivity that is lower than either would have with the absence of the other; an indication that the phonon-phonon interaction of the longitudinal and

flexural modes produces scattering resulting in the thermal conductivity seen for the DWNT.

Thermal conductivity of functionalized carbon nanotubes

The influence of united atom models of phenyl groups on the thermal conductivity of 200 nm SWNTs and DWNTs is studied. Figure 18 shows the results of thermal conductivity for different densities of functionalization. Thermal conductivity for a (10,10) SWNT experiences a significant drop with only 0.25% of its atoms functionalized. The lowest thermal conductivity is shown for 1% functionalization. The introduction of united atoms creates a phonon scattering site, which effectively reduces the phonon MFP in the SWNT, thus decreasing thermal conductivity. The results are similar to those found by Padgett and Brenner for (10,10) SWNT [35]. In contrast, the (10,10)@(19,10) DWNT's thermal conductivity increases with a small amount of functionalization and only begins to decrease between 5% and 10% functionalization densities, but only slightly. The DWNT has an additional wall that can contribute to thermal transport, so thermal conductivity is not expected to experience a decrease like that of the SWNT. The increase of thermal conductivity, however, for the SWNT and DWNT is unexpected. The increase for the SWNT can be attributed to the increased functionalization causing the SWNT to approach the behavior of a DWNT. The functionalizing atoms in the case of the DWNT initially increase thermal conductivity, because the additional atoms restrict the flexural motion of the DWNT, which increases thermal conductivity when the longitudinal mode is unrestricted as mentioned in the previous section. The influence of restricted flexural motion can be corroborated by the thermal conductivity when the functionalization atoms are held fixed on the SWNT

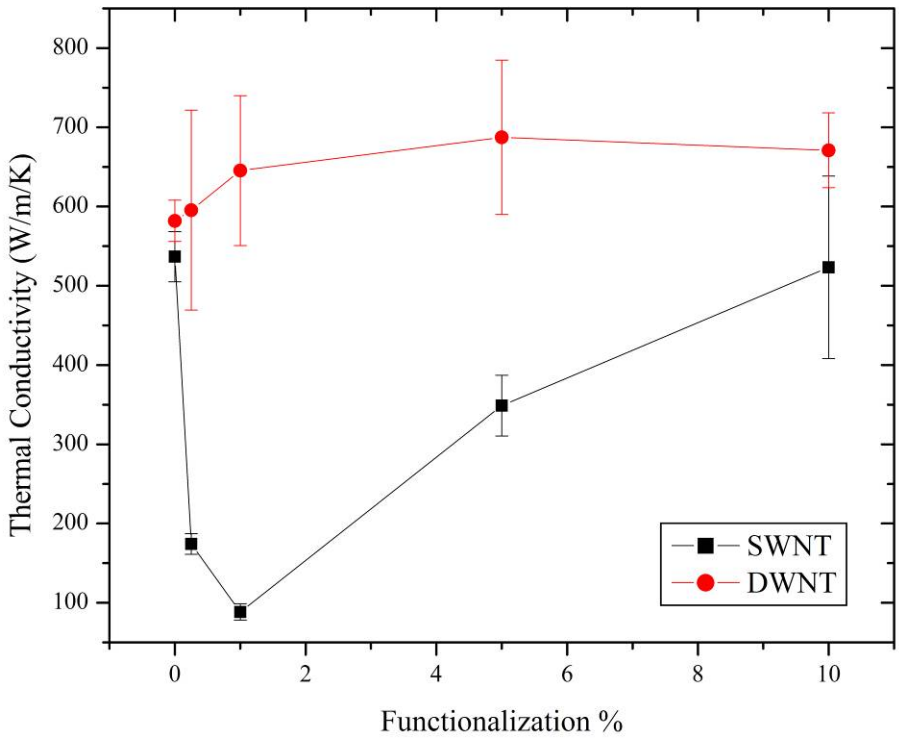

Figure 18 Thermal conductivity of a (10,10) SWNT and (10,10)@(19,10) DWNT at different functionalization densities of a phenyl united atom

(Figure 19). When the functionalizing atoms are fixed, thermal conductivity increases in a manner similar to the DWNT with mobile atoms, but quickly begins to decrease. Small percentages of functionalization are beneficial to restricting flexural motion in the SWNT; however, as the amount of fixed functionalizing atoms increase they produce a larger scattering influence by inhibiting the phonon MFP. In the case of mobile and fixed functionalizing atoms at 10%, thermal conductivity for the SWNT is the same, which is an indication the increased functionalization is influencing the SWNT's thermal conductivity to approach that of the DWNT.

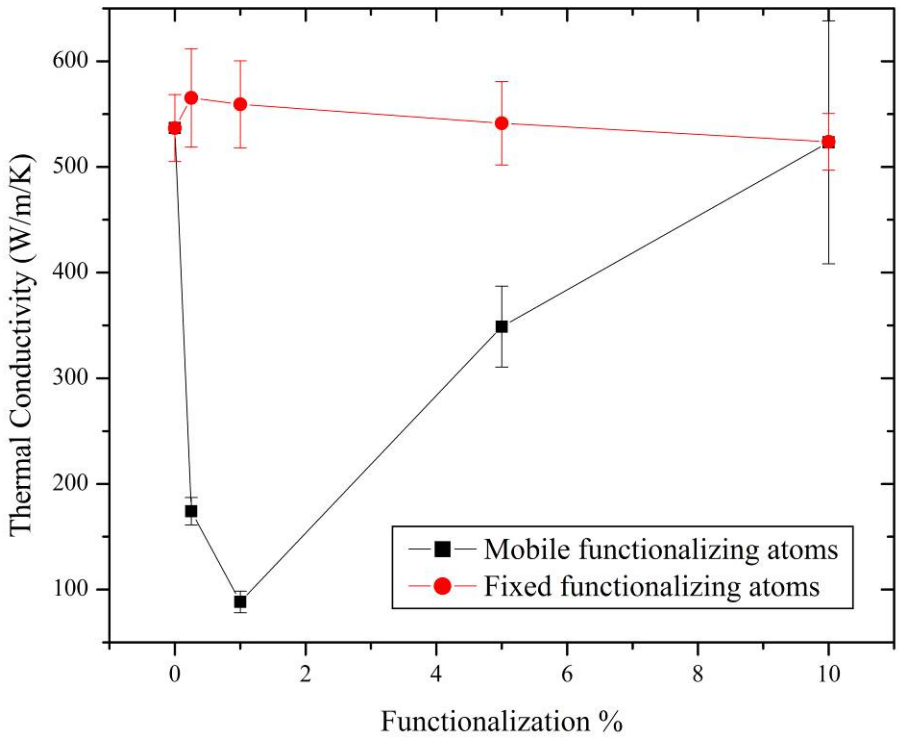

Figure 19 Thermal conductivity of (10,10) SWNT when the functionalizing atoms are mobile and fixed.

The influence on thermal conductivity of a 200 nm (10,10) SWNT is shown as the value of the Lennard-Jones parameter σ is varied. When σ is small the functionalizing atoms has an equilibrium position that can be closer to the CNT, the influence of σ is stronger when the distance is smaller. As σ increases and, consequently, the equilibrium position is further away the interaction with the CNT begins to weaken. Thermal conductivity is shown in Figure 20 for a 1% functionalized (10,10) SWNT. The error is large in this measurement since the functionalizing atoms are mobile and can move between the regions used to produce the temperature gradient during the simulation. The general trend that can be deduced from the thermal conductivity is a decrease as σ increases. When the value of σ is small and it has a stronger interaction with the SWNT,

the flexural modes are restricted allowing a larger thermal conductivity; however, as σ increases its influence is weaker and it become a scattering site disrupting the phonon MFP in the SWNT.

Table 7. Mean-square Vibrational amplitudes for 200 nm functionalized SWNTs with Various Functalization Densities

Density of Functionalization	$\langle u_r^2 \rangle$ (A^2)	$\langle u_\theta^2 \rangle$ (rad^2)	$\langle u_z^2 \rangle$ (A^2)
0%	24.037	0.16173	4.7263
0.25%	10.006	0.53713	0.71162
1%	33.893	0.21437	1.0755
5%	25.766	0.65069	11.129
10%	14.732	0.017392	1.8167

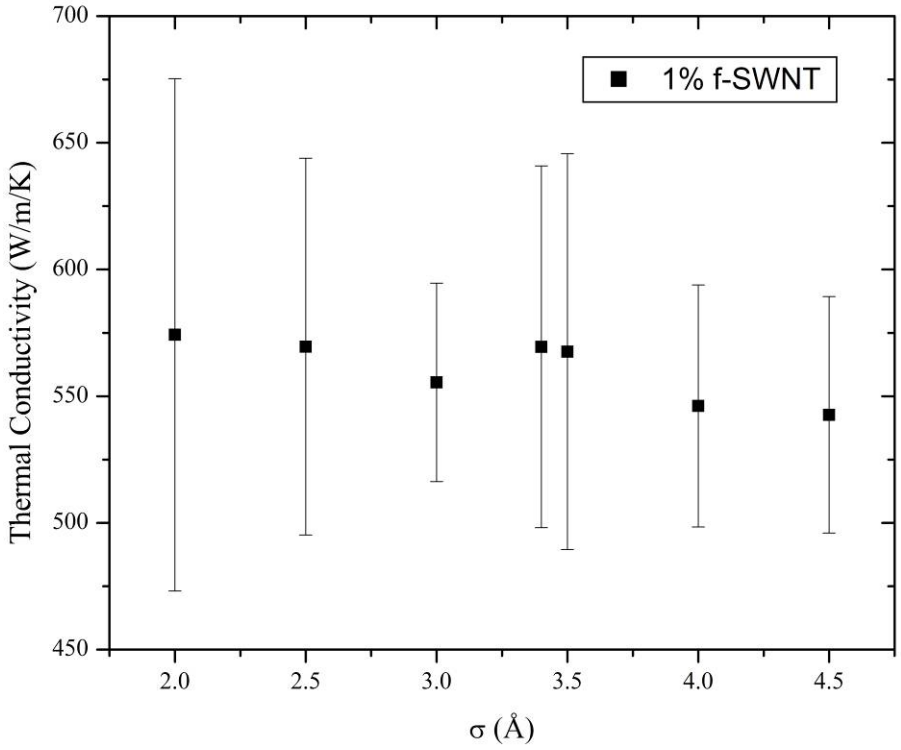

Figure 20 Thermal conductivity of (10,10) SWNT as the Lennard-Jones parameter σ is varied

Results from varying ε are not shown, because no substantial change in thermal conductivity was observed. This result is not surprising when the Lennard-Jones potential is considered. When the first derivative of the Lennard-Jones potential is considered with respect to ε, the following equation results

$$\frac{\partial U}{\partial \varepsilon} = 4\left[\frac{\sigma^{12}}{r^{12}} - \frac{\sigma^{6}}{r^{6}}\right] \tag{5.2}$$

The slope of the potential as ε is varied is a constant, so no large changes in thermal conductivity should result by changing ε. When the first derivative of the Lennard-Jones potential is considered with respect to σ, the following equation results

$$\frac{\partial U}{\partial \sigma} = 4\varepsilon\left[12\frac{\sigma^{11}}{r^{12}} - 12\frac{\sigma^{12}}{r^{13}} - 6\frac{\sigma^{5}}{r^{6}} + 6\frac{\sigma^{6}}{r^{7}}\right] \tag{5.3}$$

The slope indicates that shape of the potential changes when varying σ. The value of σ will, therefore, model the strengthening and weakening of the bond between the CNT and the united atoms.

Table 8. Mean-square Vibrational amplitudes for 200 nm 1% functionalized SWNT with Various σ Values

σ (A^2)	$<u_r^2>$ ($Å^2$)	$<u_\theta^2>$ (rad^2)	$<u_z^2>$ ($Å^2$)
2.0	13.883	0.25255	4.4366
2.5	8.1334	0.41734	4.8955
3.0	21.848	0.13979	12.441
3.5	6.1615	0.29029	3.4952
4.0	5.6616	0.32959	6.4162
4.5	10.185	0.23802	3.2807

Thermal Conductivity in Graphene

Thermal conductivity of graphene is show in Figure 21 for graphene confined in each vibrational direction (longitudinal, transverse, and flexural). Graphene can be considered an unrolled SWNT. Since graphene is 2-D versus the 3-D CNT, the two materials cannot be directly compared; however, graphene does serve as a model for the behavior of a SWNT with no torsional or radial breathing modes. The thermal conductivities show a similar trend in the length-dependence as the CNTs studied. The thermal conductivity values, however, are larger for graphene when compared to CNTs of a similar length in Figure 14. Since the CNT has additional phonon modes, the phonon-phonon interactions cause additional scattering not present in graphene [66]. The results of the NEMD simulation are comparable to those reported by others [54]. Of the single modes' thermal conductivity, the flexural mode shows the lowest overall; however, the result would be a low estimation, since the flexural mode does incorporate longitudinal motion, as well. The longitudinal and transverse modes have thermal conductivities lower than unrestricted graphene, which is due to the lack of modes to contribute to energy transport as mentioned earlier. With combinations containing two modes, the flexural mode appears to introduce phonon-phonon interactions that do not enhance thermal conductivity. Thermal conductivity increases from that observed with only the flexural mode, since the other two modes add phonon modes; however, the thermal conductivity is less than the result of the longitudinal or transverse mode alone. The out of plane motion of the flexural mode leads to a shorter MFP in the graphene, because the forces between the surrounding atoms is altered as the atoms are cause to move closer together due to the interatomic potential. Furthermore, the influence of the

flexural mode can be noticed when comparing thermal conductivities of unrestricted graphene to the combination of longitudinal and transverse modes: thermal conductivity is larger for the two mode combination, since there is no disruptive out of plane motion.

The behavior of the graphene is beneficial in understanding thermal transport in the CNT. Since torsional and radial breathing modes are not present in graphene, it can be speculated that modes that incorporate longer wavelength phonons with increasing length dominate thermal conductivity in both graphene and CNTs. Because the CNT's interatomic potential limits the vibrational motion of the atoms for the torsional and radial breathing modes, the larger influence on thermal conductivity will come from longitudinal and flexural modes, which will have a larger range of vibrational motion and also longer wavelengths of phonons.

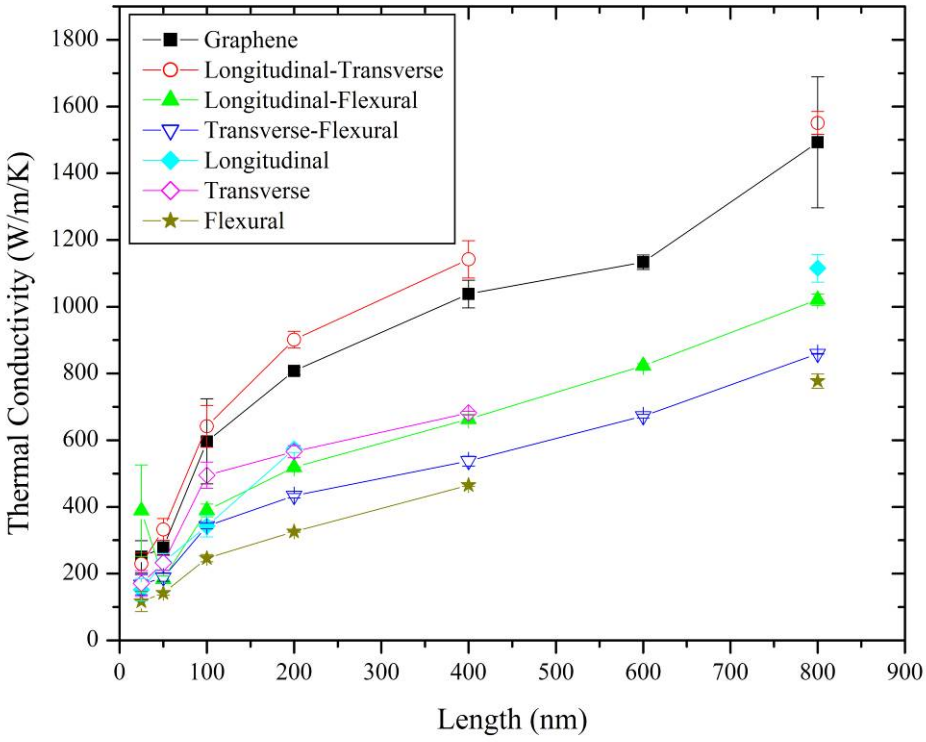

Figure 21 Thermal conductivity of graphene that is confined in various directions.

CHAPTER VI

CONCLUSIONS

Non-equilibrium MD simulations are used to investigate the influence of individual phonon on vibrational modes on the thermal conductivity in SWNTs and DWNTs. Additionally, functionalized CNTs are modeled using united atom models of phenyl to investigate the influence of functionalization on the vibrational modes and graphene confined in various directions is studied. Unlike previous studies that show thermal conductivity converging at short sample lengths, thermal conductivity of (10,10) and (19,10) SWNTs and (10,10)@(19,10) DWNTs is shown to continue increasing beyond 800 nm. Using the DWNT to confine the motion of the SWNTs, the vibrational modes are isolated and show thermal conductivity to be largely influence by the contribution of longitudinal and flexural modes. The phonon-phonon interaction of the flexural mode and longitudinal mode, however, causes degradation to thermal conductivity of CNT. The influence of suppressing the flexural mode is also seen in the thermal conductivity of functionalized (10,10) SWNTs. Though the SWNT experiences a decrease in thermal conductivity with only a small percentage of united atom phenyl groups functionalizing it, the DWNT does not show any decrease in thermal conductivity. Unexpectedly, both functionalized CNTs experience an increase in thermal conductivity attributed to the suppression of the flexural mode. While investigating the influence on bond strength on thermal conductivity using the Lennard-Jones parameters σ and ε, thermal conductivity in SWNTs was shown to have a slight response to altering σ, which

corresponds to weakening and strengthening the bond. Thermal conductivity was higher with smaller σ values—an indication that the stronger bond was also a method of suppressing flexural motion in the SWNT. Furthermore, graphene is shown to have a thermal conductivity trends that are similar to CNTs, but higher in value since there is less phonon-phonon interaction. When confining the vibrational mode, graphene also shows the flexural mode to contribute to the degradation of conductivity.

The results show promise in using CNTs in thermal management applications. Though the SWNT cannot be functionalized for use in thermal enhancement applications, DWNTs and MWNTs offer an alternative, since their interior walls offer additional pathway to transport heat even though the exterior wall may be treated. For this reason, open-ended tubes will offer better access to the CNT's interior walls than CNTs that have capped ends. When processing CNTs longer samples will largely yield better thermal conductivity as long as the length of the system is not in the diffusive regime; therefore, processing techniques that do not break the CNT will be more desirable. Graphene shows similar disadvantages as the SWNT, since scattering can be cause by treatment; however, films of a few layers of graphene may offer advantages similar to MWNTs.

Major contributions to the field of study include

- A length-dependent study of thermal conductivity in DWNTs using MD simulations,
- Confinement of vibrational motion in MD simulations,
- Altering the Lennard-Jones potential parameters σ and ε to study their influence on thermal conductivity

Future Work

There are some extensions to this work that may offer further insight to the behavior of CNTs in thermal applications. In the current work, united atom models were utilized to study the influence of bond strength on thermal conductivity. By using an explicit atom model, a more accurate study of the influence of bond strength and atom interaction can be performed. Furthermore, the use of a interatomic potential that describes covalent bonds will yield a better picture of the scattering cause by chemical treatments to the CNT. Since the broader goal is to understand better techniques for using CNTs as fillers, future studies should extend these efforts to nanocomposite samples. Models of hydrocarbons are readily described by the covalently bonding interatomic potentials in this study. Time steps, minimization, and equilibration will require much scrutiny when moving to the nanocomposite sample.

In addition to modifing the model of the CNT, studying other materials is a route of interest as well. Graphene was only considered in small instances here, but the influence of functionalization and defects on its thermal conductivity open a new direction for study. Also, boron nitride nanotubes have received consideration in thermal studies. Understanding the phonon behavior in theses materials offer a method of comparison to CNTs.

APPENDIX A

SIMULATION SCRIPTS

TubeGen Script

The following is a script that generates 150 unit cells of a (10,10) SWNT and outputs the results to a file named *data.cnt.*

```
set relax_tube yes
set format xyz
set units angstrom
set element1 C
set element2 C
set chirality 10,10
set bond 1.4210
set shape hexagonal
set gutter 5.0000, 5.0000, 0.0000
set cell_count 1,1,150
generate
save data.cnt
exit
```

LAMMPS script

The following LAMMPS scripts produce the thermal conductance for a 100 nm (5,5) SWNT under various conditions. LAMMPS is frequently updated; therefore, the latest version may not support the commands present in this script.

Script for Single-wall Carbon Nanotube Thermal Conductance

```
clear
log log.swnt5,5-100nm
###Simulation of thermal conductivity for a single-walled carbon nanotube###
###Initialization###
```

```
units metal
dimension 3
atom_style atomic
boundary p p p
processors 1 1 20

#Atom definition
read_data cnt/swnt8960-5,5-100nm+b.minimized
region wall1 block  INF INF INF INF INF 10 units box
region cold block INF INF INF INF 10 50 units box
region tube block INF INF INF INF 50 1050 units box
region hot block INF INF INF INF 1050 1091 units box
region wall2 block INF INF INF INF 1091 INF units box
#Settings and Simulation
pair_style tersoff
pair_coeff * * ../../LAMMPS/lammps-20Aug11/potentials/SiC.tersoff C
mass * 12
group wall1 region wall1
group wall2 region wall2
group cold region cold
group hot region hot
group tube region tube
group nowalls union cold tube hot

###EQUILIBRATION###
neighbor 2.0 bin
neigh_modify every 3 delay 3
velocity nowalls create 300.0 49284121
fix 1 nowalls nve
#dump 1 all custom 10000 dump.nemd.swnt-1000A_b tag type x y z
#dump 2 all xyz 500 dump.nemd.swnt-1000A_b.movie
variable g_ke equal ke(tube)
variable g_temp equal v_g_ke/1.5/8.617343e-5/8130
thermo 2000
thermo_style custom step temp ke etotal v_g_temp
timestep 0.001
run 200000

###NEMD###
#--CONSTANT FLUX--#
fix 3 cold heat 1 -5
fix 4 hot heat 1 5
compute coldBath cold temp
compute hotBath hot temp
thermo 2000
thermo_style custom step temp ke etotal v_g_temp c_coldBath c_hotBath
```

```
run 500000
log logs/log.data_collect-swnt5,5-100nm_b

###DATA COLLECTION###
compute KE tube ke/atom
variable temp atom c_KE[]/1.5/8.617343e-5
fix 5 tube ave/spatial 200 1 200 z middle 55.1 v_temp file &
        temp_profile/tmp.profile-swnt5,5-100nm_b units box
thermo 2000
thermo_style custom step temp ke etotal v_g_temp c_coldBath c_hotBath
run 500000
```

Script for Double-wall Carbon Nanotube Thermal Conductance

```
clear
log log.dwnt10,10-100nm-both
##Simulation for a double-walled CNT##
###INITIALIZATION###
units metal
dimension 3
boundary p p p
atom_style atomic

###ATOM DEFINITION###
pair_style hybrid tersoff lj/cut 5.0
read_data cnt/dwnt46656-10,10-100nm+b.minimized
mass * 12.0

###REGION DEFINITION###
region wall1 block  INF INF INF INF INF 7.9 units box
region cold block INF INF INF INF 7.9 76 units box
region tube block INF INF INF INF 76 1076 units box
region hot block INF INF INF INF 1076 1144 units box
region wall2 block INF INF INF INF 1144 INF units box

###SETTINGS###
pair_coeff  * * tersoff ../../LAMMPS/lammps-20Aug11/potentials/SiC.tersoff C C
pair_coeff 1 2 lj/cut 0.0048 3.851

###GROUP DEFINITIONS###
group one type 1
group two type 2
group wall1 region wall1
group wall2 region wall2
group cold region cold
group hot region hot
group tube region tube
group nowalls union tube cold hot

###EQUILIBRATION###
neighbor 2.0 bin
neigh_modify every 3 delay 3
timestep 0.001
fix 1 nowalls nve
velocity nowalls create 300.0 1211984
thermo 2000
thermo_style custom step temp ke etotal
run 500000
```

```
###NEMD###
fix 3 cold heat 4 -5
fix 4 hot heat 4 5
compute coldBath cold temp
compute hotBath hot temp
thermo 2000
thermo_style custom step temp ke etotal c_coldBath c_hotBath
run 500000
log logs/log.data_collect-dwnt10,10-100nm+b

###DATA COLLECTION###
compute ke nowalls ke/atom
variable temp atom c_ke/1.5/8.617343e-5
fix 5 all ave/spatial 200 1 200 z center 58.25 v_temp file &
        temp_profile/temp.profile-dwnt10,10-100nm_b units box
fix 7 one ave/spatial 200 1 200 z center 58.25 v_temp file &
        temp_profile/temp.profile-dwnt10,10-100nm_b-int units box
fix 9 two ave/spatial 200 1 200 z center 58.25 v_temp file &
        temp_profile/temp.profile-dwnt10,10-100nm_b-ext units box
thermo 2000
thermo_style custom step temp ke etotal c_coldBath c_hotBath
run 500000
```

Script for Double-wall Carbon Nanotube with Interior Wall Heated

```
clear
log log.dwnt10,10-100nm-int
##Simulation for a double-walled CNT##
###INITIALIZATION###
units metal
dimension 3
boundary p p p
atom_style atomic

###ATOM DEFINITION###
pair_style hybrid tersoff lj/cut 5.0
read_data cnt/dwnt46656-10,10-100nm+b.minimized
mass * 12.0

###REGION DEFINITION###
region wall1 block  INF INF INF INF INF 7.9 units box
region cold block INF INF INF INF 7.9 76 units box
region tube block INF INF INF INF 76 1076 units box
region hot block INF INF INF INF 1076 1144 units box
region wall2 block INF INF INF INF 1144 INF units box
region cold_inner cylinder z 0 0 7 7.9 76 units box
region cold_entire cylinder z 0 0 12 7.9 76 units box
region hot_inner cylinder z 0 0 7 1076 1144 units box
region hot_entire cylinder z 0 0 12 1076 1144 units box

###SETTINGS###
pair_coeff  * * tersoff ../../LAMMPS/lammps20Aug11/potentials/SiC.tersoff C C
pair_coeff 1 2 lj/cut 0.0048 3.851

###GROUP DEFINITIONS###
group one type 1
group two type 2
group wall1 region wall1
group wall2 region wall2
group cold region cold
group hot region hot
group tube region tube
group cold_entire region cold_entire
group hot_entire region hot_entire
group cold_inner region cold_inner
group hot_inner region hot_inner
group nowalls union tube cold hot

###EQUILIBRATION###
```

```
neighbor 2.0 bin
neigh_modify every 3 delay 3
timestep 0.001
fix 1 nowalls nve
velocity nowalls create 300.0 1211984
thermo 2000
thermo_style custom step temp ke etotal
run 500000

###NEMD###
fix 3 cold_inner heat 4 -5
fix 4 hot_inner heat 4 5
compute coldBath cold_inner temp
compute hotBath hot_inner temp
thermo 2000
thermo_style custom step temp ke etotal c_coldBath c_hotBath
run 500000
log logs/log.data_collect_int-dwnt10,10-100nm_b

###DATA COLLECTION###
compute ke nowalls ke/atom
variable temp atom c_ke/1.5/8.617343e-5
fix 5 all ave/spatial 200 1 200 z center 58.25 v_temp file &
        temp_profile/temp.profile_intt-dwnt10,10-100nm_b units box
fix 7 one ave/spatial 200 1 200 z center 58.25 v_temp file &
        temp_profile/temp.profile_int-dwnt10,10-100nm_b-int units box
fix 9 two ave/spatial 200 1 200 z center 58.25 v_temp file &
        temp_profile/temp.profile_int-dwnt10,10-100nm_b-ext units box
thermo 2000
thermo_style custom step temp ke etotal c_coldBath c_hotBath
run 500000
```

Script for Double-wall Carbon Nanotube with Interior Wall Heated

```
clear
log log.dwnt10,10-100nm-ext
##Simulation for a double-walled CNT##
###INITIALIZATION###
units metal
dimension 3
boundary p p p
atom_style atomic

###ATOM DEFINITION###
pair_style hybrid tersoff lj/cut 8.0
read_data cnt/dwnt46656-10,10-100nm+b.minimized
mass * 12.0

###REGION DEFINITION###
region wall1 block  INF INF INF INF INF 7.9 units box
region cold block INF INF INF INF 7.9 76 units box
region tube block INF INF INF INF 76 1076 units box
region hot block INF INF INF INF 1076 1144 units box
region wall2 block INF INF INF INF 1144 INF units box
region cold_inner cylinder z 0 0 7 7.9 76 units box
region cold_entire cylinder z 0 0 12 7.9 76 units box
region hot_inner cylinder z 0 0 7 1076 1144 units box
region hot_entire cylinder z 0 0 12 1076 1144 units box

###SETTINGS###
pair_coeff  * * tersoff ../../LAMMPS/lammps-20Aug11/potentials/SiC.tersoff C C
pair_coeff 1 2 lj/cut 0.0048 3.851

###GROUP DEFINITIONS###
group one type 1
group two type 2
group wall1 region wall1
group wall2 region wall2
group cold region cold
group hot region hot
group tube region tube
group cold_entire region cold_entire
group hot_entire region hot_entire
group cold_inner region cold_inner
group hot_inner region hot_inner
group nowalls union tube cold hot
group chiller subtract cold_entire cold_inner
group heater subtract hot_entire hot_inner
```

```
###EQUILIBRATION###
neighbor 2.0 bin
neigh_modify every 3 delay 3
timestep 0.001
fix 1 nowalls nve
velocity nowalls create 300.0 1211984
thermo 2000
thermo_style custom step temp ke etotal
run 500000

###NEMD###
fix 3 chiller heat 4 -5
fix 4 heater heat 4 5
compute coldBath chiller temp
compute hotBath heater temp
thermo 2000
thermo_style custom step temp ke etotal c_coldBath c_hotBath
run 500000
log logs/log.data_collect_ext-dwnt10,10-100nm_b

###DATA COLLECTION###
compute ke nowalls ke/atom
variable temp atom c_ke/1.5/8.617343e-5
fix 5 all ave/spatial 200 1 200 z center 58.25 v_temp file &
        temp_profile/temp.profile_ext-dwnt10,10-100nm_b units box
fix 7 one ave/spatial 200 1 200 z center 58.25 v_temp file &
        temp_profile/temp.profile_ext-dwnt10,10-100nm_b-int units box
fix 9 two ave/spatial 200 1 200 z center 58.25 v_temp file &
        temp_profile/temp.profile_ext-dwnt10,10-100nm_b-ext units box
thermo 2000
thermo_style custom step temp ke etotal c_coldBath c_hotBath
run 500000
```

Script for Double-wall Carbon Nanotube with Exterior Wall Moving

```
clear
log log.dwnt10,10-100nm-ext_only
##Simulation for a double-walled CNT##
###INITIALIZATION###
units metal
dimension 3
boundary p p p
atom_style atomic

###ATOM DEFINITION###
pair_style hybrid tersoff lj/cut 8.0
read_data cnt/dwnt46656-10,10-100nm+b.minimized
mass * 12.0

###REGION DEFINITION###
region wall1 block  INF INF INF INF INF 7.9 units box
region cold block INF INF INF INF 7.9 76 units box
region tube block INF INF INF INF 76 1076 units box
region hot block INF INF INF INF 1076 1144 units box
region wall2 block INF INF INF INF 1144 INF units box
region cold_inner cylinder z 0 0 7 7.9 76 units box
region cold_entire cylinder z 0 0 12 7.9 76 units box
region hot_inner cylinder z 0 0 7 1076 1144 units box
region hot_entire cylinder z 0 0 12 1076 1144 units box

###SETTINGS###
pair_coeff  * * tersoff ../../LAMMPS/lammps-20Aug11/potentials/SiC.tersoff C C
pair_coeff 1 2 lj/cut 0.0048 3.851

###GROUP DEFINITIONS###
group one type 1
group two type 2
group wall1 region wall1
group wall2 region wall2
group cold region cold
group hot region hot
group tube region tube
group cold_entire region cold_entire
group hot_entire region hot_entire
group cold_inner region cold_inner
group hot_inner region hot_inner
group nowalls union tube cold hot
group chiller subtract cold_entire cold_inner
group heater subtract hot_entire hot_inner
```

```
group sample subtract two wall1 wall2

###EQUILIBRATION###
neighbor 2.0 bin
neigh_modify every 3 delay 3
timestep 0.001
fix 1 sample nve
velocity nowalls create 300.0 1211984
thermo 2000
thermo_style custom step temp ke etotal
run 200000

###NEMD###
fix 3 chiller heat 4 -5
fix 4 heater heat 4 5
compute coldBath chiller temp
compute hotBath heater temp
thermo 2000
thermo_style custom step temp ke etotal c_coldBath c_hotBath
run 500000
log logs/log.data_collect_ext_only-dwnt10,10-100nm_b

###DATA COLLECTION###
compute ke nowalls ke/atom
variable temp atom c_ke/1.5/8.617343e-5
fix 5 all ave/spatial 200 1 200 z center 58.25 v_temp file &
        temp_profile/temp.profile_ext_only-dwnt10,10-100nm_b units box
fix 7 one ave/spatial 200 1 200 z center 58.25 v_temp file &
        temp_profile/temp.profile_ext_only-dwnt10,10-100nm_b-int units box
fix 9 two ave/spatial 200 1 200 z center 58.25 v_temp file &
        temp_profile/temp.profile_ext_only-dwnt10,10-100nm_b-ext units box
thermo 2000
thermo_style custom step temp ke etotal c_coldBath c_hotBath
run 500000
```

Script for Double-wall Carbon Nanotube with Interior Wall Moving

```
clear
log log.dwnt10,10-100nm-int_only
##Simulation for a double-walled CNT##
###INITIALIZATION###
units metal
dimension 3
boundary p p p
atom_style atomic

###ATOM DEFINITION###
pair_style hybrid tersoff lj/cut 5.0
read_data cnt/dwnt46656-10,10-100nm+b.minimized
mass * 12.0

###REGION DEFINITION###
region wall1 block  INF INF INF INF INF 7.9 units box
region cold block INF INF INF INF 7.9 76 units box
region tube block INF INF INF INF 76 1076 units box
region hot block INF INF INF INF 1076 1144 units box
region wall2 block INF INF INF INF 1144 INF units box
region cold_inner cylinder z 0 0 7 7.9 76 units box
region cold_entire cylinder z 0 0 12 7.9 76 units box
region hot_inner cylinder z 0 0 7 1076 1144 units box
region hot_entire cylinder z 0 0 12 1076 1144 units box

###SETTINGS###
pair_coeff  * * tersoff ../../LAMMPS/lammps-20Aug11/potentials/SiC.tersoff C C
pair_coeff 1 2 lj/cut 0.0048 3.851

###GROUP DEFINITIONS###
group one type 1
group two type 2
group wall1 region wall1
group wall2 region wall2
group cold region cold
group hot region hot
group tube region tube
group cold_entire region cold_entire
group hot_entire region hot_entire
group cold_inner region cold_inner
group hot_inner region hot_inner
group nowalls union tube cold hot
group sample subtract one wall1 wall2
```

```
###EQUILIBRATION###
neighbor 2.0 bin
neigh_modify every 3 delay 3
timestep 0.001
fix 1 sample nve
velocity nowalls create 300.0 1211984
thermo 2000
thermo_style custom step temp ke etotal
run 500000

###NEMD###
fix 3 cold_inner heat 4 -5
fix 4 hot_inner heat 4 5
compute coldBath cold_inner temp
compute hotBath hot_inner temp
thermo 2000
thermo_style custom step temp ke etotal c_coldBath c_hotBath
run 500000
log logs/log.data_collect_int_only-dwnt10,10-100nm_b

###DATA COLLECTION###
compute ke nowalls ke/atom
variable temp atom c_ke/1.5/8.617343e-5
fix 5 all ave/spatial 200 1 200 z center 58.25 v_temp file &
        temp_profile/temp.profile_int_only-dwnt10,10-100nm_b units box
fix 7 one ave/spatial 200 1 200 z center 58.25 v_temp file &
        temp_profile/temp.profile_int_only-dwnt10,10-100nm_b-int units box
fix 9 two ave/spatial 200 1 200 z center 58.25 v_temp file &
        temp_profile/temp.profile_int_only-dwnt10,10-100nm_b-ext units box
thermo 2000
thermo_style custom step temp ke etotal c_coldBath c_hotBath
run 500000
```

Script for Functionalized Single-wall Carbon Nanotube

```
clear
log log.fswnt10,10-200nm-1%
##Simulation for a double-walled CNT##

###INITIALIZATION###
units metal
dimension 3
boundary p p p
atom_style atomic

###ATOM DEFINITION###
pair_style hybrid tersoff lj/cut 5.0
read_data /workspace/walkere1/func33844-10,10-200nm+b-1%-1.minimized

mass 1 12.0
mass 2 77.0

###SETTINGS###
pair_coeff  * * tersoff ../../local/lammps-4Dec11/potentials/SiC.tersoff C NULL
pair_coeff 1 2 lj/cut 0.0035 3.7755
pair_coeff 2 2 lj/cut 0.0026 3.7

###GROUP DEFINITIONS###
group one type 1
group two type 2
group wall1 id <= 260
group wall2 id <> 33261 33520
group cold id <> 261 520
group hot id <> 33001 33260
group tube id <> 521 33000
group sample union tube cold hot
group nowalls union tube cold hot two

###EQUILIBRATION###
neighbor 2.0 bin
neigh_modify every 3 delay 3

variable m loop 3
label loop1
if "$m > 4" then "jump script/in.fswnt200-1 exitloop1"
minimize 0.0 1e-8 100000 1000000
fix 2 all nve
velocity all set 0.0 0.0 0.0 units box
run 100
```

```
unfix 2
next m
jump script/in.fswnt200-1 loop1
label exitloop1

timestep 0.001
fix 1 nowalls nve
velocity nowalls create 300.0 1211984

variable g_ke equal ke(sample)
variable g_temp equal v_g_ke/1.5/8.6173743e-5/33000

thermo 2000
thermo_style custom step temp ke etotal v_g_temp
run 50000

label test
if "(${g_temp} > 297.0) && (${g_temp} < 303.0)" then &
 "jump script/in.fswnt200-1 break" &
 else &
 "velocity sample scale 300.0" "run 10000" "jump script/in.fswnt200-1 test"
label break

reset_timestep 0
###DATA COLLECTION###
dump 1 tube custom 10 /workspace/walkere1/dump25_1/*.fswnt200-1.dos id type xu yu
zu vx vy vz
dump_modify 1 sort id
dump 2 two custom 10 /workspace/walkere1/dump25_1/fatoms/*.fatoms200-1.dos id
type xu yu zu vx vy vz
dump_modify 2 sort id
run 50000
```

Script for Functionalized Double-wall Carbon Nanotube

```
clear
log log.funcd10,10-200nm-1%
##Simulation for a double-walled CNT##

###INITIALIZATION###
units metal
dimension 3
boundary p p p
atom_style atomic

###ATOM DEFINITION###
pair_style hybrid tersoff lj/cut 5.0
read_data cnt/func93782-10,10-200nm+b-1%-2.minimized

mass * 12.0
mass 3 77.0

###REGION DEFINITION###
region wall1 block  INF INF INF INF INF 16.3 units box
region cold block INF INF INF INF 16.3 152 units box
region tube block INF INF INF INF 152 2152 units box
region hot block INF INF INF INF 2152 2288 units box
region wall2 block INF INF INF INF 2288 INF units box

###SETTINGS###
pair_coeff  * * tersoff ../lammps-7Apr11/potentials/SiC.tersoff C C NULL
pair_coeff 1 2 lj/cut 0.0048 3.851
pair_coeff 1 3 lj/cut 0.0010 3.55
pair_coeff 2 3 lj/cut 0.0010 3.55
pair_coeff 3 3 lj/cut 0.0026 3.7

###GROUP DEFINITIONS###
group one type 1
group two type 2
group three type 3

group wall1 region wall1
group wall2 region wall2
group cold region cold
group hot region hot
group tube region tube
group nowalls union tube cold hot

###EQUILIBRATION###
```

```
neighbor 2.0 bin
neigh_modify every 3 delay 3

timestep 0.001
fix 1 nowalls nve
velocity nowalls create 300.0 1211984

dump 1 all xyz 5000 /workspace/walkere1/fdwnt10,10-200nm+b-1.xyz

thermo 2000
thermo_style custom step temp ke etotal
run 100000

###NEMD###
fix 3 cold heat 5 -2
fix 4 hot heat 5 2

compute coldBath cold temp
compute hotBath hot temp

thermo 2000
thermo_style custom step temp ke etotal c_coldBath c_hotBath
run 500000

log logs/log.data_collect-funcd10,10-200nm+b-1%
###DATA COLLECTION###
compute ke nowalls ke/atom
variable temp atom c_ke/1.5/8.617343e-5

fix 5 all ave/spatial 200 1 200 z center 116.25 v_temp file &
 temp_profile/temp.profile-fdwnt10,10-200nm_b-1% units box
fix 7 one ave/spatial 200 1 200 z center 116.25 v_temp file &
 temp_profile/temp.profile-fdwnt10,10-200nm_b-1%-int units box
fix 9 two ave/spatial 200 1 200 z center 116.25 v_temp file &
 temp_profile/temp.profile-fdwnt10,10-200nm_b-1%-ext units box
fix 11 three ave/spatial 200 1 200 z center 116.25 v_temp file &
 temp_profile/temp.profile-fdwnt10,10-200nm_b-1%-func units box

thermo 2000
thermo_style custom step temp ke etotal c_coldBath c_hotBath
run 1000000
```

Script for Graphene Thermal Conductance

```
clear
log log.graphene-10,10-100nm
#Simulation of thermal conductivity for a single-walled carbon nanotube

#Initialization
units metal
atom_style atomic
boundary p p p
#processors 1 1 20

#Atom definition
read_data crystal/graphene32520-10,10-200nm

#Settings and Simulation
pair_style tersoff
pair_coeff * * ../../../../../LAMMPS/lammps-20Aug11/potentials/SiC.tersoff C

mass 1 12

neighbor 2.0 bin
neigh_modify every 3 delay 3

timestep 0.001

thermo 2000
thermo_style custom step temp ke etotal pe

variable m loop 3
label loop1
if "$m > 3" then "jump script/in.graphene100 exitloop1"
minimize 0.0 1e-8 100000 1000000
fix 2 all nve
velocity all set 0.0 0.0 0.0 units box
run 100
unfix 2
next m
jump script/in.graphene100 loop1
label exitloop1

velocity all create 300.0 1211984
fix 1 all nve

#dump 1 all custom 10000 dump.nemd.swnt-100nm tag type x y z
#dump 2 all xyz 10000 dump.nemd.swnt-100nm.movie
```

```
run 200000
reset_timestep 0

fix KEswap all thermal/conductivity 50 z 20 swap 20

compute KE all ke/atom
variable temp atom c_KE/1.5/8.617343e-5
fix 3 all ave/spatial 2000 1 2000 z lower 100 &
        v_temp file temp.profile-graphene10,10-100nm units box

thermo 2000
thermo_style custom step temp ke etotal f_KEswap
run 1000000
```

Script for Bilayer Graphene Thermal Conductance

```
clear
log log.bilayer-10,10-100nm
#Simulation of thermal conductivity for a single-walled carbon nanotube

#Initialization
units metal
atom_style atomic
boundary p p p
#processors 1 1 20

#Atom definition
read_data crystal/bilayer65040-10,10-200nm

#Settings and Simulation
pair_style hybrid tersoff lj/cut 5.0
pair_coeff * * tersoff ../../../../../LAMMPS/lammps-20Aug11/potentials/SiC.tersoff C C
pair_coeff 1 2 lj/cut 0.0048 3.851

mass * 12

group one type 1
group two type 2

neighbor 2.0 bin
neigh_modify every 3 delay 3

timestep 0.001

thermo 2000
thermo_style custom step temp ke etotal pe

variable m loop 3
label loop1
if "$m > 3" then "jump script/in.bilayer100 exitloop1"
minimize 0.0 1e-8 100000 1000000
fix 2 all nve
velocity all set 0.0 0.0 0.0 units box
run 100
unfix 2
next m
jump script/in.bilayer100 loop1
label exitloop1

velocity all create 300.0 1211984
```

```
fix 1 one nve

#dump 1 all custom 10000 dump.nemd.swnt-100nm tag type x y z
dump 2 all xyz 10000 /scratch/walkere1/bilayer-lower_nve-100nm.xyz

run 200000
#reset_timestep 0

fix KEswap one thermal/conductivity 50 z 20 swap 20

compute KE all ke/atom
variable temp atom c_KE/1.5/8.617343e-5
fix 3 all ave/spatial 2000 1 2000 z lower 100 &
          v_temp file temp.profile-bilayer10,10-100nm units box
fix 4 one ave/spatial 2000 1 2000 z lower 100 &
         v_temp file temp.profile-bilayer10,10-100nm-lower units box
fix 5 two ave/spatial 2000 1 2000 z lower 100 &
         v_temp file temp.profile-bilayer10,10-100nm-upper units box

thermo 2000
thermo_style custom step temp ke etotal f_KEswap
run 1000000
```

APPENDIX B

RAW THERMAL CONDUCTIVITY DATA

Table 9 Thermal Conductivity of CNTs

Length (nm)	(5,5) SWNT (W/m/K)	Error	(10,10) SWNT (W/m/K)	Error	(19,10) SWNT (W/m/K)	Error	(10,10)@(19,10) DWNT (W/m/K)	Error
25	170.99666	29.33374	140.92182	25.59983	173.48272	28.05006	166.25662	31.90126
50	263.3963	41.29698	306.49064	31.53486	290.84733	42.07485	293.75032	29.72806
100	414.76315	49.20131	449.55952	41.31526	433.57847	36.55526	534.54005	71.91429
200	518.40133	72.92037	536.72015	31.66977	574.50649	40.30291	581.87192	26.02082
400	890.863	81.4537	622.53426	38.06833	887.08157	45.22056	638.4812	22.85769
600	937.19795	49.63509	711.39758	45.01525	933.3214	45.34244	742.42844	38.02399
800	1115.24086	110.26017	863.52858	69.77223	951.27301	45.89825	899.54076	58.91302
1000	--	--	1244.87024	114.25777	1171.14969	69.14745	987.46402	36.02984
1500	--	--	1454.66234	212.38729			850.02047	53.87179
2000			2186.11663	401.99703			1290.39803	139.27782
3000			4187.7945	1126.254			3655.57925	582.18407
4000			7563.15786	2618.58304	5937.70465	2142.66414		

Table 10 Thermal Conductivity of DWNTs Using Different Heating Schemes

Length (nm)	External Wall Heated (W/m/K)	Error	Internal Wall Heated (W/m/K)	Error	External Wall Moving (W/m/K)	Error	Internal Wall Moving (W/m/K)	Error
25	174.02127	36.05994	156.34753	28.46671	294.11473	45.91583	--	--
50	299.73404	27.73143	249.78176	19.35103	440.59229	56.78718	407.15119	-6.89746
100	527.00717	47.79234	455.49764	49.64906	727.46782	92.42369	585.95557	81.84783
200	617.78415	31.32403	552.65748	35.14281	929.68075	69.71034	713.17754	118.13679
400	648.87296	21.37998	636.38556	36.06449	--	--	929.60363	46.18447
600	--	---	---	--	1101.92208	72.44247	1030.78639	39.39937
800	899.03945	54.28724	896.00096	61.68708	1214.25229	58.43104	1173.12427	136.86581
1000	985.13865	94.00774	1037.53665	95.85505	1193.74363	49.84031	1297.96399	172.0879
1500	1030.99676	103.37286	1024.90467	107.24647	1193.74363	573.10988	1723.72712	334.06992
2000	1321.81351	135.62123	1306.62894	139.16186	1898.58288	137.40801	3141.46624	553.68101

Table 11 Thermal Conductivity of CNTs with One Mode Suppressed

Length (nm)	Longitudinal, Breathing, and Torsional Modes (W/m/K)	Error	Breathing, Torsional, and Flexural Modes (W/m/K)	Error
25	294.11473	45.91583	78.7913	9.76106
50	440.59229	56.78718	138.13702	17.40752
100	727.46782	92.42369	303.61062	75.75204
200	929.68075	69.71034	395.07055	83.36899
400	--	--	501.63948	20.06164
600	1101.92208	72.44247	739.52962	54.57531
800	1214.25229	58.43104	1044.28212	123.19404
1000	1193.74363	49.84031	1407.35106	215.27427
1500	1193.74363	573.10988	--	--
2000	1898.58288	137.40801	4546.14521	1268.90696

Table 12 Thermal Conductivity of CNTs with Two or More Modes Suppressed

Length (nm)	Longitudinal and Breathing Modes (W/m/K)	Error	Longitudinal and Torsional Modes (W/m/K)	Error	Breathing and Torsional Modes (W/m/K)	Error	Torsional Mode (W/m/K)	Error
25	229.66166	32.72364	--	--	125.20432	10.48268	100.18326	22.90195
50	332.28888	32.802	407.15119	-6.89746	147.62718	13.91429	151.10052	23.51796
100	641.80627	62.51569	585.95557	81.84783	245.0224	9.99427	207.03857	23.89742
200	901.27375	25.36579	713.17754	118.13679	310.14138	9.11714	268.11855	30.22596
400	1142.00279	55.82339	929.60363	46.18447	669.57918	77.35612	369.88955	59.29056
600	--	--	1030.78639	39.39937	500.4295	35.01759	427.8313	7.98397
800	1550.65732	34.31116	1173.12427	136.86581	675.65468	64.4527	639.51819	11.47011
1000	--	--	1297.96399	172.0879			--	--
1500	--	--	1723.72712	334.06992			--	--
2000	--	--	3141.46624	553.68101			1551.07041	443.4958

Table 13 Thermal Conductivity of Functionalized CNTs at Various Percentages

Functionalization Percentage	Mobile Functionalization Atoms				Immobile Functionalization Atoms	
	SWNT (W/m/K)	Error	DWNT (W/m/K)	Error	SWNT (W/m/K)	Error
0	536.72015	31.66977	581.87192	26.02082	536.72015	31.66977
0.25	174.11974	13.01021	595.38774	126.05238	565.36151	46.6133
1	88.33585	10.24321	645.31359	94.51452	559.17637	41.28186
5	348.83527	38.28959	687.39737	97.50571	541.33424	39.52961
10	523.3027	115.03968	670.86783	47.18866	523.69198	26.78142

Table 14 Thermal Conductivity of Functionalized SWNTs for Various Values of the Lennard-Jones Parameter σ

σ (Å)	SWNT (W/m/K)	Error
2	574.22653	101.12719
2.5	569.52532	74.36083
3	555.46585	39.16571
3.4	569.46076	71.39115
3.5	567.58945	78.11221
4	546.14878	47.77027
4.5	542.66908	46.68799

Table 15 Thermal Conductivity of Graphene with Three and Two Vibrational Modes Present

Length (nm)	Longitudinal, Transverse, and Flexural Modes (W/m/K)	Error	Longitudinal and Transverse Modes (W/m/K)	Error	Longitudinal and Flexural Modes (W/m/K)	Error	Transverse and Flexural Modes (W/m/K)	Error
25	250.69929	47.9866	229.66166	32.72364	388.95823	-137.2689	167.13773	30.82557
50	277.71046	21.36809	332.28888	32.802	183.44887	9.78646	188.9923	11.81183
100	596.38053	127.58018	641.80627	62.51569	389.48291	18.94428	342.70239	8.61946
200	807.38218	11.05847	901.27375	25.36579	519.18396	-0.31629	433.47442	-6.65034
400	1038.21187	41.42254	1142.00279	55.82339	663.27047	-10.88052	537.63303	-14.93018
600	1133.35293	-21.75835	--	--	823.41171	-6.26143	672.15897	-5.32454
800	1492.8481	196.35843	1550.65732	34.31116	1021.15709	17.20757	859.10264	1.07983

Table 16 Thermal Conductivity of Graphene with One Vibrational Mode Present

Length (nm)	Longitudinal Mode (W/m/K)	Error	Transverse Mode (W/m/K)	Error	Flexural Mode (W/m/K)	Error
25	151.69509	33.54289	170.53952	38.73513	116.70738	30.48095
50	235.20953	25.68199	232.24978	22.14694	141.92742	5.78283
100	342.40458	32.67994	495.10012	39.77051	246.3465	10.99773
200	573.22958	9.42386	565.70171	-18.13764	325.74059	-1.68378
400	--	--	681.898	-4.91729	465.0279	3.65241
600	--	--	--	--	--	--
800	1115.1365	41.26508	--	--	777.11087	21.42393

REFERENCES

[1] S. Iijima, "Helical microtubules of graphitic carbon," *Nature*, vol. 354, pp. 56–58, 1991.

[2] "Heat Transfer," *Heat Exchanger Design*, 2011. [Online]. Available: http://heatexchanger-design.com/2011/03/07/heat-transfer-2/.

[3] C. Kittel and H. Kroemer, *Thermal Physics*, Second ed. W. H. Freeman, 1980.

[4] J. Fourier, *The Analytical Theory of Heat*. London: Cambridge, 1878.

[5] W. D. J. Callister, *Materials Science and Engineering: An Introduction*, 7th ed. Wiley, 2006.

[6] C. Kittel, *Introduction to Solid State Physics*, 8th ed. Wiley, 2004.

[7] R. F. Pierret, *Advanced Semiconductor Fundamentals*, 2nd ed. Prentice Hall, 2002.

[8] G. Chen, *Nanoscale Energy Transport and Conversion: A Parallel Treatment of Electrons, Molecules, Phonons, and Photons*. Oxford University Press, USA, 2005.

[9] W. S. Capinski, H. J. Maris, T. Ruf, M. Cardona, K. Ploog, and D. S. Katzer, "Thermal-conductivity measurements of GaAs/AlAs superlattices using a picosecond optical pump-and-probe technique," *Phys. Rev. B*, vol. 59, no. 12, p. 8105, Mar. 1999.

[10] S. Reich, C. Thomsen, and J. Maultzsch, *Carbon Nanotubes: Basic Concepts and Physical Properties*. Wiley-VCH, 2004.

[11] X. Lu and Z. Chen, "Curved Pi-Conjugation, Aromaticity, and the Related Chemistry of Small Fullerenes (," *Chem. Rev.*, vol. 105, no. 10, pp. 3643–3696, 2005.

[12] M. A. Osman and D. Srivastava, "Temperature dependence of the thermal conductivity of single-wall carbon nanotubes," *Nanotechnology*, vol. 12, no. 1, pp. 21–24, 2001.

[13] J. Hone, M. Whitney, C. Piskoti, and A. Zettl, "Thermal conductivity of single-walled carbon nanotubes," *Phys. Rev. B*, vol. 59, no. 4, p. R2514–R2516, Jan. 1999.

[14] D. J. Yang, Q. Zhang, G. Chen, S. F. Yoon, J. Ahn, S. G. Wang, Q. Zhou, Q. Wang, and J. Q. Li, "Thermal conductivity of multiwalled carbon nanotubes," *Phys. Rev. B*, vol. 66, no. 16, p. 165440, Oct. 2002.

[15] J. Hone, M. C. Llaguno, N. M. Nemes, A. T. Johnson, J. E. Fischer, D. A. Walters, M. J. Casavant, J. Schmidt, and R. E. Smalley, "Electrical and thermal transport properties of magnetically aligned single wall carbon nanotube films," *Applied Physics Letters*, vol. 77, no. 5, p. 666, 2000.

[16] P. Kim, L. Shi, A. Majumdar, and P. L. McEuen, "Thermal Transport Measurements of Individual Multiwalled Nanotubes," *Phys. Rev. Lett.*, vol. 87, no. 21, p. 215502, Oct. 2001.

[17] M. Fujii, X. Zhang, H. Xie, H. Ago, K. Takahashi, T. Ikuta, H. Abe, and T. Shimizu, "Measuring the Thermal Conductivity of a Single Carbon Nanotube," *Phys. Rev. Lett.*, vol. 95, no. 6, p. 065502, 2005.

[18] C. Yu, L. Shi, Z. Yao, D. Li, and A. Majumdar, "Thermal Conductance and Thermopower of an Individual Single-Wall Carbon Nanotube," *Nano Letters*, vol. 5, no. 9, pp. 1842–1846, 2005.

[19] E. Pop, D. Mann, Q. Wang, K. Goodson, and H. Dai, "Thermal Conductance of an Individual Single-Wall Carbon Nanotube above Room Temperature," *Nano Letters*, vol. 6, no. 1, pp. 96–100, Jan. 2006.
[20] J. P. Small, L. Shi, and P. Kim, "Mesoscopic thermal and thermoelectric measurements of individual carbon nanotubes," *Solid State Communications*, vol. 127, no. 2, pp. 181–186, Jul. 2003.
[21] J. Hone, M. Whitney, and A. Zettl, "Thermal conductivity of single-walled carbon nanotubes," *Synthetic Metals*, vol. 103, pp. 2498–2499, 1999.
[22] S. Berber, Y.-K. Kwon, and D. Tomanek, "Unusually High Thermal Conductivity of Carbon Nanotubes," *Phys. Rev. Lett.*, vol. 84, no. 20, p. 4613, May 2000.
[23] J. Che, T. Cagin, and W. A. Goddard III, "Thermal conductivity of carbon nanotubes," *Nanotechnology*, vol. 11, no. 2, pp. 65–69, 2000.
[24] P. Kim, "Mesoscopic thermal transport and energy dissipation in carbon nanotubes," *Physica B: Condensed Matter*, vol. 323, no. 1–4, pp. 67–70, Oct. 2002.
[25] S. Maruyama, "A molecular dynamics simulation of heat conduction in finite length SWNTs," *Physica B: Condensed Matter*, vol. 323, no. 1–4, pp. 193–195, Oct. 2002.
[26] W. Zhang, Z. Zhu, F. Wang, T. Wang, L. Sun, and Z. Wang, "Chirality dependence of the thermal conductivity of carbon nanotubes," *Nanotechnology*, vol. 15, no. 8, pp. 936–939, Aug. 2004.
[27] G. Zhang and B. Li, "Thermal conductivity of nanotubes revisited: Effects of chirality, isotope impurity, tube length, and temperature," *The Journal of Chemical Physics*, vol. 123, no. 11, p. 114714, 2005.
[28] T. Y. Choi, D. Poulikakos, J. Tharian, and U. Sennhauser, "Measurement of thermal conductivity of individual multiwalled carbon nanotubes by the 3-ω method," *Applied Physics Letters*, vol. 87, no. 1, p. 013108, 2005.
[29] M. Grujicic, G. Cao, and W. N. Roy, "Computational analysis of the lattice contribution to thermal conductivity of single-walled carbon nanotubes," *Journal of Materials Science*, vol. 40, no. 8, pp. 1943–1952, 2005.
[30] T.-Y. Choi, D. Poulikakos, J. Tharian, and U. Sennhauser, "Measurement of the Thermal Conductivity of Individual Carbon Nanotubes by the Four-Point Three-ω Method," *Nano Lett.*, vol. 6, no. 8, pp. 1589–1593, 2006.
[31] M. C. Llaguno, "Thermal conductivity of single wall carbon nanotubes: Diameter and annealing dependence," 2001, vol. 591, pp. 384–387.
[32] Z. L. Wang, D. W. Tang, X. B. Li, X. H. Zheng, W. G. Zhang, L. X. Zheng, Y. T. Zhu, A. Z. Jin, H. F. Yang, and C. Z. Gu, "Length-dependent thermal conductivity of an individual single-wall carbon nanotube," *Applied Physics Letters*, vol. 91, no. 12, p. 123119, Sep. 2007.
[33] J. X. Cao, X. H. Yan, Y. Xiao, Y. Tang, and J. W. Ding, "Exact study of lattice dynamics of single-walled carbon nanotubes," *Phys. Rev. B*, vol. 67, no. 4, p. 045413, Jan. 2003.
[34] J. X. Cao, X. H. Yan, Y. Xiao, and J. W. Ding, "Thermal conductivity of zigzag single-walled carbon nanotubes: Role of the umklapp process," *Phys. Rev. B*, vol. 69, no. 7, p. 073407, Feb. 2004.

[35] C. W. Padgett and D. W. Brenner, “Influence of Chemisorption on the Thermal Conductivity of Single-Wall Carbon Nanotubes,” *Nano Lett.*, vol. 4, no. 6, pp. 1051–1053, Jun. 2004.
[36] R. Saito, R. Matsuo, T. Kimura, G. Dresselhaus, and M. S. Dresselhaus, “Anomalous potential barrier of double-wall carbon nanotube,” *Chemical Physics Letters*, vol. 348, no. 3–4, pp. 187–193, Nov. 2001.
[37] W. Guo and Y. Guo, “Energy Optimum Chiralities of Multiwalled Carbon Nanotubes,” *Journal of the American Chemical Society*, vol. 129, no. 10, pp. 2730–2731, Mar. 2007.
[38] E. Mamontov, C. J. Burnham, S.-H. Chen, A. P. Moravsky, C.-K. Loong, N. R. de Souza, and A. I. Kolesnikov, “Dynamics of water confined in single- and double-wall carbon nanotubes,” *The Journal of Chemical Physics*, vol. 124, no. 19, p. 194703–194703–6, May 2006.
[39] M. Dequesnes, S. V. Rotkin, and N. R. Aluru, “Calculation of pull-in voltages for carbon-nanotube-based nanoelectromechanical switches,” *Nanotechnology*, vol. 13, no. 1, pp. 120–131, Feb. 2002.
[40] S. U. S. Choi, Z. G. Zhang, W. Yu, F. E. Lockwood, and E. A. Grulke, “Anomalous thermal conductivity enhancement in nanotube suspensions,” *Appl. Phys. Lett.*, vol. 79, no. 14, p. 2252, 2001.
[41] M. J. Biercuk, M. C. Llaguno, M. Radosavljevic, J. K. Hyun, A. T. Johnson, and J. E. Fischer, “Carbon nanotube composites for thermal management,” *Appl. Phys. Lett.*, vol. 80, no. 15, p. 2767, 2002.
[42] H. Xie, H. Lee, W. Youn, and M. Choi, “Nanofluids containing multiwalled carbon nanotubes and their enhanced thermal conductivities,” *Journal of Applied Physics*, vol. 94, no. 8, p. 4967, 2003.
[43] S. T. Huxtable, D. G. Cahill, S. Shenogin, L. Xue, R. Ozisik, P. Barone, M. Usrey, M. S. Strano, G. Siddons, M. Shim, and P. Keblinski, “Interfacial heat flow in carbon nanotube suspensions,” *Nature Materials*, vol. 2, no. 11, pp. 731–734, Oct. 2003.
[44] A. Moisala, Q. Li, I. A. Kinloch, and A. H. Windle, “Thermal and electrical conductivity of single- and multi-walled carbon nanotube-epoxy composites,” *Composites Science and Technology*, vol. 66, no. 10, pp. 1285–1288, Aug. 2006.
[45] C.-W. Nan, Z. Shi, and Y. Lin, “A simple model for thermal conductivity of carbon nanotube-based composites,” *Chemical Physics Letters*, vol. 375, no. 5–6, pp. 666–669, Jul. 2003.
[46] F. H. Gojny, M. H. G. Wichmann, B. Fiedler, I. A. Kinloch, W. Bauhofer, A. H. Windle, and K. Schulte, “Evaluation and identification of electrical and thermal conduction mechanisms in carbon nanotube/epoxy composites,” *Polymer*, vol. 47, no. 6, pp. 2036–2045, Mar. 2006.
[47] A. A. Balandin, S. Ghosh, W. Bao, I. Calizo, D. Teweldebrhan, F. Miao, and C. N. Lau, “Superior Thermal Conductivity of Single-Layer Graphene,” *Nano Lett.*, vol. 8, no. 3, pp. 902–907, 2008.
[48] P. G. Klemens, “Theory of the A-Plane Thermal Conductivity of Graphite,” *Journal of Wide Bandgap Materials*, vol. 7, no. 4, pp. 332–339, Apr. 2000.
[49] P. G. Klemens, “Theory of Thermal Conduction in Thin Ceramic Films,” *Internation Journal of Thermophysics*, vol. 22, no. 1, p. 265–175, 2001.

[50] D. L. Nika, E. P. Pokatilov, A. S. Askerov, and A. A. Balandin, "Phonon thermal conduction in graphene: Role of Umklapp and edge roughness scattering," *Phys. Rev. B*, vol. 79, no. 15, p. 155413, Apr. 2009.
[51] D. L. Nika, S. Ghosh, E. P. Pokatilov, and A. A. Balandin, "Lattice thermal conductivity of graphene flakes: Comparison with bulk graphite," *Applied Physics Letters*, vol. 94, no. 20, p. 203103–203103–3, May 2009.
[52] "Grüneisen parameter." [Online]. Available: http://en.wikipedia.org/wiki/Gr%C3%BCneisen_Parameter. [Accessed: 17-Feb-2012].
[53] J. Hu, X. Ruan, and Y. P. Chen, "Thermal Conductivity and Thermal Rectification in Graphene Nanoribbons: A Molecular Dynamics Study," *Nano Lett.*, vol. 9, no. 7, pp. 2730–2735, 2009.
[54] Z. Guo, D. Zhang, and X.-G. Gong, "Thermal conductivity of graphene nanoribbons," *Applied Physics Letters*, vol. 95, no. 16, p. 163103–163103–3, Oct. 2009.
[55] S. Ghosh, I. Calizo, D. Teweldebrhan, E. P. Pokatilov, D. L. Nika, A. A. Balandin, W. Bao, F. Miao, and C. N. Lau, "Extremely high thermal conductivity of graphene: Prospects for thermal management applications in nanoelectronic circuits," *Applied Physics Letters*, vol. 92, no. 15, p. 151911–151911–3, Apr. 2008.
[56] P. Zhang, Y. Huang, P. H. Geubelle, P. A. Klein, and K. C. Hwang, "The elastic modulus of single-wall carbon nanotubes: a continuum analysis incorporating interatomic potentials," *International Journal of Solids and Structures*, vol. 39, no. 13–14, pp. 3893–3906, Jun. 2002.
[57] S. J. Stuart, A. B. Tutein, and J. A. Harrison, "A reactive potential for hydrocarbons with intermolecular interactions," *J. Chem. Phys.*, vol. 112, no. 14, p. 6472, 2000.
[58] J. Tersoff, "New empirical approach for the structure and energy of covalent systems," *Phys. Rev. B*, vol. 37, no. 12, p. 6991, Apr. 1988.
[59] D. W. Brenner, "Empirical potential for hydrocarbons for use in simulating the chemical vapor deposition of diamond films," *Phys. Rev. B*, vol. 42, no. 15, p. 9458, Nov. 1990.
[60] F. Muller-Plathe, "A simple nonequilibrium molecular dynamics method for calculating the thermal conductivity," *The Journal of Chemical Physics*, vol. 106, p. 6082, 1997.
[61] F. Muller-Plathe and D. Reith, "Cause and effect reversed in non-equilibrium molecular dynamics: an easy route to transport coefficients," *Computational and Theoretical Polymer Science*, vol. 9, no. 3–4, pp. 203–209, Dec. 1999.
[62] S. J. Plimpton, "Fast Parallel Algorithms for Short-Range Molecular Dynamics," *J Comp Phys*, vol. 117, pp. 1–19, 1995.
[63] J. T. Frey and D. J. Doren, *TubeGen*. Newark, DE: University of Delaware, 2005.
[64] H. A. Rafizadeh, "An analytical-potential approach to the lattice dynamics of graphite," *Physica*, vol. 74, no. 1, pp. 135–150, May 1974.
[65] L. Lindsay and D. A. Broido, "Optimized Tersoff and Brenner empirical potential parameters for lattice dynamics and phonon thermal transport in carbon nanotubes and graphene," *Phys. Rev. B*, vol. 81, no. 20, p. 205441, May 2010.

[66] L. Lindsay, D. A. Broido, and N. Mingo, "Diameter dependence of carbon nanotube thermal conductivity and extension to the graphene limit," *Phys. Rev. B*, vol. 82, no. 16, p. 161402, Oct. 2010.
[67] E. González Noya, D. Srivastava, L. A. Chernozatonskii, and M. Menon, "Thermal conductivity of carbon nanotube peapods," *Phys. Rev. B*, vol. 70, no. 11, p. 115416, 2004.
[68] M. G. Holland, "Analysis of Lattice Thermal Conductivity," *Phys. Rev.*, vol. 132, no. 6, pp. 2461–2471, Dec. 1963.
[69] J. Callaway, "Model for Lattice Thermal Conductivity at Low Temperatures," *Phys. Rev.*, vol. 113, no. 4, pp. 1046–1051, Feb. 1959.
[70] E. A. Walker and D. G. Walker, "Influence of Vibrational Modes on Thermal Conductivity in Single-walled Carbon Nanotubes," *Submitted for Publication*.